REVIEW / SYNTHÈSE

Recent progress in spectroscopy of tungsten[1]

A. Kramida

Abstract: This contribution reviews experimental and theoretical work on spectroscopy of tungsten published since the last critical compilation of the energy levels and spectral lines of highly ionized tungsten (Kramida and Shirai. *At. Data Nucl. Data Tables*, **95**, 305 (2009)). Since then, 18 new experimental studies were published, which resulted in new identifications and (or) significantly improved wavelengths of spectral lines and energy levels of Li-like through As-like and Pm-like tungsten. A few tens of theoretical studies of tungsten spectra were published since 2008. A number of them report on high-precision calculations of energy levels, transition wavelengths, and radiative rates for tungsten spectra, such as neutral tungsten, Yb-like, Rh-like through Rb-like, Ag-like, Ga-like, Zn-like, Ni-like, Ca-like, Al-like, Mg-like, Na-like, Ne-like, B-like, Be-like, and Li-like. These developments are reviewed. Based on new experimental data, systematic errors are removed from some of the earlier measurements. Some new data are obtained by analyzing publications of other authors. Based on new published theoretical data, some old experimental results were confirmed and assessed. Revised and extended tables of energy levels and spectral lines of highly ionized tungsten are presented.

PACS Nos: 32.10.Fn, 32.30.–r, 32.30.Jc, 32.30.Rj

Résumé : Nous passons ici en revue les travaux expérimentaux et théoriques sur la spectroscopie du tungstène, qui ont été publiés depuis la dernière compilation systématique des niveaux d'énergie et des raies spectrales du tungstène hautement ionisé (Kamida et Shirai. *At. Data Nucl. Data Tables*, **95**, 305 (2009)). Depuis, 18 nouvelles études expérimentales ont été publiées, qui ont résulté en de nouvelles identifications et une amélioration significative des longueurs d'onde des raies et de l'énergie des niveaux des ions de tungstène allant du type Li jusqu'aux types As et Pm. Quelques dizaines études théoriques sur le tungstène ont été publiées depuis 2008. Certaines d'entre elles rapportent des calculs de haute précision de niveaux d'énergie, de longueurs d'onde de transitions et de taux radiatifs pour des spectres de tungstène, neutre et ionisé de types Yb, de Rh à Rb, Ag, Ga, Zn, Ni, Ca, Al, Mg, Na, Ne, B, Be et Li. Nous les passons en revue. Les mesures récentes ont permis d'éliminer certaines erreurs systématiques des mesures antérieures. Certains nouveaux résultats viennent de l'analyse de publications d'autres auteurs. Les nouveaux résultats théoriques ont permis de confirmer des résultats expérimentaux antérieurs dont l'identification restait incertaine. Nous présentons des tables nouvelles et étendues des niveaux d'énergie et des raies spectrales du tungstène hautement ionisé.

[Traduit par la Rédaction]

1. Introduction

An extensive review and critical compilation of experimental data on highly-ionized tungsten was recently made by Kramida and Shirai [1]. This compilation included data published until the beginning of 2008. Since then, several new tens of studies of various tungsten spectra have been published. They can be divided into three categories:

1. New experimental observations of emission spectra [2–16];
2. New theoretical interpretations of previously observed spectra [17–20];
3. Purely theoretical studies [21–50].

These three categories will be discussed in the following sections, and an index of studied subjects (measured or calculated wavelengths or energies, energy level classifications, Zeeman effect, transition probabilities, etc.) will be given at the end of the present paper. The highest priority is given to the studies that extend the knowledge of atomic structure. This review is not intended to present a comprehensive coverage of work related to plasma diagnostics and theoretical modeling of spectra. Its main purpose is to extend the reference data for energy levels and wavelengths of tungsten spectra.

Complete revised tables of critically compiled energy levels and spectral lines of Li-like through As-like and Pm-like tung-

Received 16 September 2010. Accepted 25 March 2011. Published at www.nrcresearchpress.com/cjp on 20 May 2011.

A. Kramida. National Institute of Standards and Technology, 100 Bureau Drive, Gaithersburg, MD 20899-8422, USA.

E-mail for correspondence: Alexander.Kramida@nist.gov.

[1]This review is part of a Special Issue on the 10th International Colloquium on Atomic Spectra and Oscillator Strengths for Astrophysical and Laboratory Plasmas.

Fig. 1. Dependence of wavelengths of the $2s_{1/2}$–$2p_{1/2,\,3/2}$ transitions along the Li-like isoelectronic sequence. The measured wavelength of the $2s_{1/2}$–$2p_{3/2}$ transition for tungsten ($Z = 74$) is from Clementson et al. [7]. The wavelength of the unobserved $2s_{1/2}$–$2p_{3/2}$ transition is based on interpolation of calculations of Blundell [51].

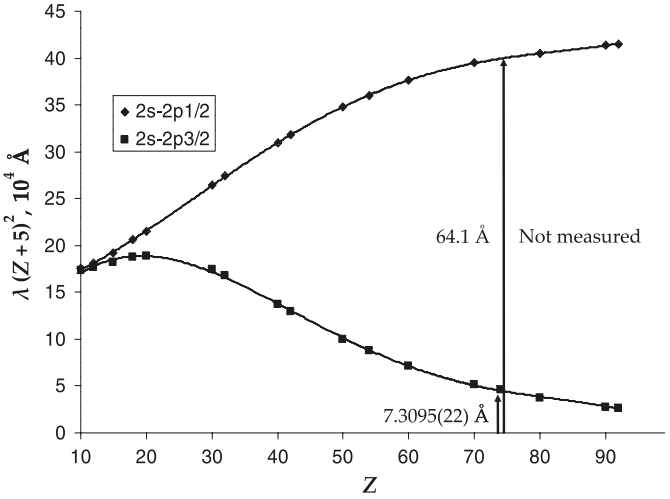

sten, as assessed from the new studies reviewed in the present paper are included in the online Supplementary Data.[2]

2. New experimental observations

2.1. Li-like through Ne-like (W LXXII–LXV) [6, 7, 10]

Podpaly et al. [10] reported the first identification of 11 resonance transitions in F-like through Li-like W of the type $2s_{1/2}$–$2p_{3/2}$ in the soft X-ray region 1.7–1.9 keV (6.6–7.3 Å). These measurements were made at the SuperEBIT facility of the Lawrence Livermore National Laboratory (LLNL) with a flat-crystal spectrometer. The line widths were limited by the resolution of the position-sensitive proportional counter, used as a detector, and amounted to approximately 1.5 eV (FWHM). The total uncertainties of the measured energies of the peaks were dominated by the calibration uncertainties and varied in the range 1.0–2.3 eV, corresponding to the wavelength uncertainties of 0.004–0.008 Å.[3] Podplay et al. [10], in their Fig. 1, depicted a broad-range spectrum of F-like through Li-like W between 1 and 12 keV, taken with a microcalorimeter. This spectrum contains about 200 spectral lines with rich structures in the ranges 8–12 and 2.3–3.8 keV, corresponding to the $n = 2 - n = 3$ and $n = 3 - n = 4$ transitions, respectively. These transition arrays have not been investigated so far.

Figure 1 shows the dependence of the wavelengths of the two resonance transitions $2s_{1/2}$–$2p_{1/2,3/2}$ along the Li-like isoelectronic sequence. This behavior is similar to the Na-like resonance doublet discussed by Gillaspy et al. [11] (see Sect. 2.2). However, in heavy Li-like ions the relativistic effects are much more pronounced than in Na-like ions, so that for Li-like W^{71+} the ratio of the two wavelengths is close to nine.

The short-wavelength $2s_{1/2}$–$2p_{3/2}$ transition was measured by Podpaly et al. [10] at 7.305(4) Å. Clementson et al. [7] refined the wavelength to be 7.3095(22) Å. The long-wavelength $2s_{1/2}$–$2p_{1/2}$ transition has not been observed so far. However, its wavelength can be determined with reasonable accuracy by interpolating the differences between observed and calculated wavelengths along the isoelectronic sequence. The most extensive calculations of the energies of the $n = 2$ levels of Li-like ions were made by Yerokhin et al. [52]. Although they calculated the quantum-electrodynamic (QED) contributions to the energies for only a few members of the sequence, their Table IV gives values of electronic structure contributions to the energies for all Li-like ions from Li to U. By interpolating the differences of experimental energies from these theoretical values, it is possible to derive empirical values of the remaining corrections (dominated by QED contributions) to the energies of all Li-like ions. Table 1 shows the details of this interpolation. Experimental values of the energies of the $2p_{1/2}$ levels were taken from previous publications [53–69].

The differences between the experimental energies and theoretical electronic-structure contributions (column 6 of Table 1) were fitted with a 6th degree polynomial shown below:

$$E_{\mathrm{interp}} - E_{\mathrm{th}}^{\mathrm{es}} = 218.4 - 60.858\,Z + 6.74431\,Z^2 - 0.441\,9931\,Z^3 + 0.002\,103\,911\,Z^4 - 4.170\,945 \times 10^{-5}\,Z^5 + 1.326\,973 \times 10^{-7}\,Z^6\,[\mathrm{cm}^{-1}] \quad (1)$$

The residuals of the fit and 68% confidence-level intervals are shown in Fig. 2.

From this fitting, the wavelength of the $2s_{1/2}$–$2p_{1/2}$ transition in Li-like W^{71+} is 64.140(12) Å.

As mentioned above, the measurements of Podpaly et al. [10] were made with a flat-crystal spectrometer. The electron-beam energy was 103.2 keV. Clementson et al. [7] made a set of measurements in the same wavelength range with a microcalorimeter spectrograph and with beam energies varying from 23.5 to 122 keV. Although the instrumental resolution of the microcalorimeter (7 eV) was significantly worse than that of the crystal spectrometer (1.5 eV), the much greater signal-to-noise ratio allowed Clementson et al. [7] to measure the energies of isolated peaks with lower uncertainties and identify several additional lines of B-like W LXX, C-like W LXIX, O-like W LXVII, F-like W LXVI, and Ne-like W LXV. The magnetic-dipole $2s^22p^5\,{}^2P^o_{3/2}$–$\,{}^2P^o_{1/2}$ transition of F-like W LXVI at 8.927(4) Å and electric-quadrupole $2s^22p^2\ {}^3P_0$–$\,{}^3P_2$ transition of C-like W LXIX at 8.672(3) Å, measured in that work, are particularly important for the ITER plasma diagnostics. The identifications were supported by collisional-radiative modeling with atomic data generated by the Flexible Atomic Code (FAC) [71] and by comparison of the experimental and modeled spectra at different electron-beam energies. Clementson's thesis [6] contains more details of this experiment and describes the modeling procedure. The relative intensities of the lines given in the tables (see the online Supplementary Data) were derived from the spectrograms given in the thesis [6].[2]

[2]Supplementary data are available with the article through the journal Web site (nrcresearchpress.com).
[3]All uncertainties given in the present paper are intended to be on the level of one standard deviation, corresponding to the 68% level of confidence.

Table 1. Interpolation of excitation energies of the $2p_{1/2}$ levels in Li-like ions.

Z	E_{exp} (cm^{-1})	Unc. (cm^{-1})	Ref.	E_{th}^{es} (cm^{-1}) [52][a]	ΔE [b] (cm^{-1})	E_{interp} (cm^{-1})	Unc. (cm^{-1})	$\delta E_{exp-interp}$ (cm^{-1})
10	128 151.9	1.8	[53]	128 294	–142	128 153	6	–1
12	160 015	3	[54]	160 282	–267	160 011	4	4
15	208 204	25	[55]	208 777	–573	208 185.1	2.2	19
18	257 019.9	2.0	[56]	258 146	–1 126	257 023.0	1.6	–3.1
19	273 501	15	[57]	274 844	–1 343	273 486.0	1.7	15
20	290 047	7	[56]	291 677	–1 631	290 052.1	2.1	–5
21	306 748	282	[58]	308 654	–1 905	306 725	3	23
22	323 557	16	[59]	325 786	–2 229	323 516	3	40
23	—	—	—	343 083	—	340 431	4	—
24	357 484	6	[60]	360 551	–3 067	357 474	5	9
25	374 706	42	[57]	378 201	–3 495	374 654	6	52
26	391 983	8	[61]	396 042	–4 059	391 976	7	7
28	427 071	9	[62]	432 341	–5 270	427 079	9	–8
29	444 850	20	[59]	450 814	–5 964	444 871	10	–21
30	462 832	24	[63]	469 520	–6 688	462 836	11	–4
32	499 264	15	[64]	507 660	–8 396	499 303	13	–39
34	536 596	20	[64]	546 852	–10 256	536 547	16	49
36	574 614	65	[65]	587 182	–12 569	574 630	18	–16
40	—	—	—	671 619	—	653 565	23	—
42	694 454	96	[59]	715 891	–21 437	694 530	30	–76
47	802 021	58	[66]	833 508	–31 486	802 010	40	11
50	870 360	61	[67]	909 336	–38 976	870 310	50	50
54	966 417	65	[67]	1 017 423	–51 006	966 450	60	–33
60	—	—	—	1 196 753	—	1 123 150	110	—
70	—	—	—	1 549 410	—	1 422 840	230	—
74	—	—	—	1 713 184	—	1 559 100	300	—
79	1 743 375	370	[68]	1 937 818	–194 443	1 743 260	350	115
80	—	—	—	1 985 170	—	1 781 700	400	—
82	1 860 318	380	[68]	2 082 748	–222 431	1 860 450	360	–132
83	—	—	—	2 132 751	—	1 900 590	360	—
90	—	—	—	2 498 543	—	2 187 970	220	—
92	2 263 555	123	[69]	2 599 738	–336 184	2 263 550	120	5

[a]From Table IV of Yerokhin et al. [52]. Conversion from atomic units to cm^{-1} was made with the value of the Rydberg constant from Mohr et al. [70].
[b]Difference between E_{exp} and E_{th}^{es}.

Fig. 2. Residuals of the polynomial fitting of excitation energies of the $2p_{1/2}$ levels of Li-like ions. The error bars represent the experimental uncertainties. The dashed curves correspond to the 68% confidence level intervals.

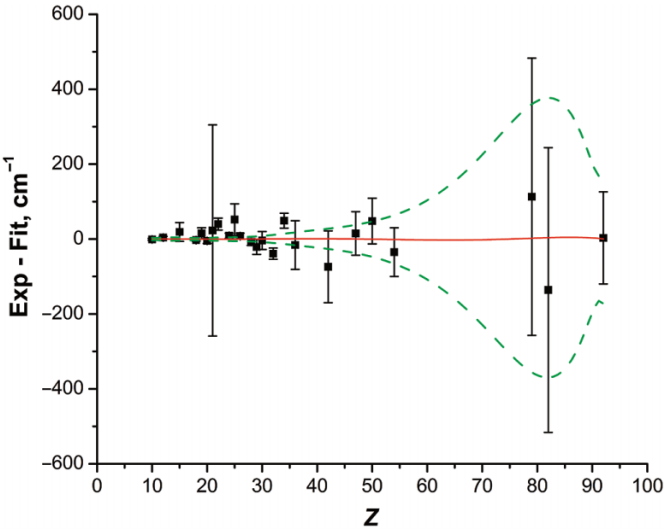

2.2. Ne-like through K-like (W LXV–LVI) [2, 11]

Gillaspy et al. [11] reported the first observation of the $3s_{1/2}$–$3p_{1/2,\ 3/2}$ resonance lines of Na-like W^{63+}. This resonance-line doublet is otherwise known as the D-lines (D_1 and D_2, corresponding to the $3s_{1/2}$–$3p_{1/2}$ and $3s_{1/2}$–$3p_{3/2}$ transitions). The measurements were made at the EBIT facility of the National Institute of Standards and Technology (NIST) with a grazing incidence spectrometer. Along with the D-lines of Na-like W^{63+}, similar D-lines were also measured for Na-line Hf, Ta, and Au. In addition, several lines of Mg-like through Si-like W, Hf, and Ta and one line of Mg-like Au were observed and measured for the first time. The statistical uncertainties of the measured wavelengths varied between 0.004 and 0.030 Å, depending on the signal-to-noise ratio, while the calibration uncertainty was about 0.015 Å. The wavelength of the D_2 line of W^{63+} ($3s_{1/2}$–$3p_{3/2}$) was measured to be 23.243(17) Å. This line was subsequently re-measured with much smaller uncertainty by Clementson and Beiersdorfer [2] (see below). For the wavelength of the D_1 line ($3s_{1/2}$–$3p_{1/2}$), Gillaspy et al. [11] determined the weighted average of their measurement and the previous one (Ralchenko et al. [72]) to be 77.700 (12) Å.

Spectra of K-like W^{55+} through Ne-like W^{64+} in the region 19 to 25 Å were investigated by Clementson and Beiersdorfer [2]. Using the LLNL SuperEBIT facility equipped with a grazing-incidence soft-X-ray spectrometer, these authors measured the wavelengths of 20 $n = 3$ to $n = 3$ transitions with uncertainties in the range of 0.005–0.01 Å. Line identifications were guided by calculations with the FAC code of Gu [71] and by comparisons with isoelectronic spectra.

2.3. K-like through Co-like (W LVI–XLVIII) [9]

Spectra of magnetic-dipole (M1) transitions within the ground configurations of Co-like W^{47+} through K-like W^{55+} were investigated by the NIST EBIT team [9] using a grazing-incidence spectrometer in the region 120–255 Å. Measurement uncertainties were about 0.03 Å. Line identifications were guided by collisional-radiative modeling with the NOMAD code [73] using atomic data calculated with the FAC code [71]. Discrimination of the lines belonging to different ionization stages was facilitated by comparisons of spectra observed at different energies of the electron beam. An interesting feature of the observed spectra was that almost all of the observed lines were due to M1 transitions. These observations provide a basis for determination of the electronic structure of the $3d^n$ ground configurations of Co-like W^{47+} through Ca-like W^{54+}.

The value of the fine-structure splitting of the $3p^63d$ ground configuration of K-like W^{55+} given in the previous compilation [1] was based on extrapolation of Ali and Kim [74]. The wavelength of the $3p^63d\ ^2D_{3/2}$–$^2D_{5/2}$ M1 transition measured by Ralchenko et al. [75], 159.61(3) Å, agreed with the value predicted by Ali and Kim, 159.585(5) Å, within the measurement uncertainty. However, the new improved measurement [9] resulted in 159.62(3) Å, which agrees with the extrapolation of Ali and Kim only marginally. In this regard, it should be noted that the small uncertainty assigned to the extrapolation of Ali and Kim in the compilation of Kramida and Shirai [1] was too optimistic. New measurements on other isoelectronic high-Z ions are needed to establish the trend along the sequence.

The FAC calculations of the energy levels of the ground configurations of Co-like W^{47+} through Ca-like W^{54+} [9] are in good agreement with the observed wavelengths of M1 transitions within these configurations. For this reason, some of these calculated energy levels are included in the tables of energy levels (see the online Supplementary Data) to complement the values found from the observed wavelengths.[2] The uncertainties of the calculated levels are estimated to be within (2–5) × 10^3 cm^{-1}. The level designations in the *jj* coupling scheme are from the same calculations.

2.4. Co-like through As-like (W XLVIII– XLII) [4, 3, 8]

Clementson et al. [4] have measured the wavelengths of the two components of the forbidden E2+M3 doublet $3d^{10}\ ^1S$ –$3d^94s\ (5/2,1/2)_{2,3}$ in Ni-like W^{46+} using a high-resolution crystal spectrometer at the LLNL SuperEBIT installation. The measured wavelengths are 7.9280(6) and 7.9374(7) Å for the E2 and M3 transitions, respectively.

The spectra of Zn-like W^{44+} through Co-like W^{47+} in the wide soft X-ray region between 3 and 12 Å (photon energies 1–4 keV) were investigated by Clementson et al. [3] using a microcalorimeter spectrometer at the LLNL SuperEBIT facility. Figure 2 of their paper gives an overview of the spectrum recorded at a beam energy of 4.0 keV. This high-resolution image can be magnified and used to determine the positions and relative intensities of all observed peaks. This is especially easy because of the roughly linear scale of the voltage response of the microcalorimeter detector versus the energy of the incident photon. Although the exact form of the voltage–energy dependence curve is non-linear and depends on the properties of the detecting pixels as well as on the electronic equipment and other elements of the set-up, the

Fig. 3. (color online). Calibration curve of the microcalorimeter detector of Clementson et al. [3] derived from Fig. 2 of their paper (see text). Small rhombs represent differences of peak positions tabulated in [3] from rough energies inferred from the linear energy scale of Fig. 2 of [3]; magenta squares represent deviations of peak energies measured by Neill et al. [76, 77] from the linear scale of Fig. 2 of [3]; green triangles represent lines of Cu-like W^{45+} present in Fig. 2 of [3], but not included in their tables; light-blue circle represents the lowest-energy peak used by Clementson et al. [3] for calibration. The error bars represent the measurement uncertainties. The solid curve is a parabola fitted to the small rhombs. The thin dashed curves represent 68% confidence limits of the fit.

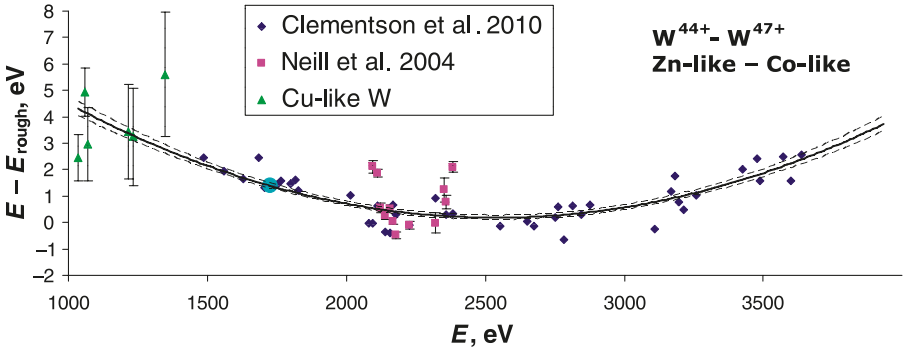

Table 2. Wavelengths of lines of Cu-like W^{45+} determined from Fig. 2 of Clementson et al. [3].

E_{obs} (eV)	λ_{obs} (Å)	λ_{prev} (Å)	Ref.	Lower level	Upper level
1038.6(5)	11.938(6)	11.959(10)	[80]	$3d^{10}4p\ ^2P^o_{1/2}$	$3d^{10}5d\ ^2D_{3/2}$
1061.9(5)	11.675(6)	11.667(10)	[80]	$3d^{10}4s\ ^2S_{1/2}$	$3d^{10}5p\ ^2P^o_{3/2}$
1071.9(5)	11.567(6)	11.570(15)	[79]	$3d^{10}4f\ ^2F^o_{7/2}$	$3d^{10}6g\ ^2G_{9/2}$
1217.7(5)	10.181(4)	10.181(15)	[79]	$3d^{10}4d\ ^2D_{5/2}$	$3d^{10}6f\ ^2F^o_{7/2}$
1237.7(5)	10.017(4)	10.024(15)	[79]	$3d^{10}4d\ ^2D_{3/2}$	$3d^{10}6f\ ^2F^o_{5/2}$
1348.6(5)	9.193(3)	9.174(16)	[78]	$3d^{10}4p\ ^2P^o_{3/2}$	$3d^94s^2\ ^2D_{5/2}$

Fig. 4. Derivation of the calibration correction for wavelengths measured by Neill et al. [76, 77]. The quantity plotted is the difference between the peak energy measured by Neill et al. and the reference value (see text). The error bars represent the uncertainties in the reference energies combined in quadrature with the stated measurement uncertainties of Neill et al. The latter are generally very small, similar to the error bars of the two phosphorus lines at 2.15 and 2.3 keV. The solid curve is a parabola fitted to the data points. The dotted curves represent the 68% confidence level bounds.

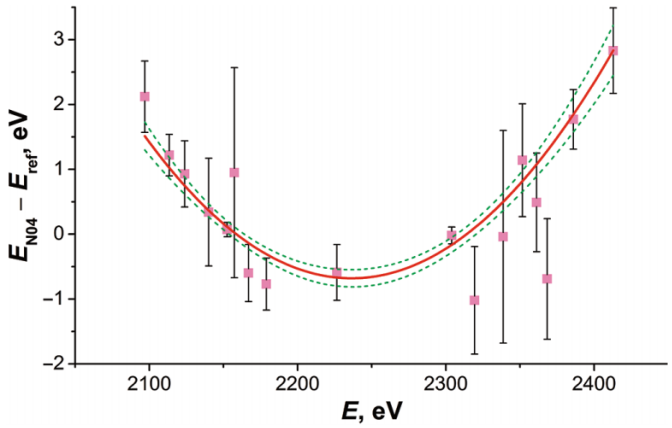

extent of the non-linearity in the photon energy range of 1–4 keV is typically on the order of only a few percent. In the work of Clementson et al. [3], the calorimeter data were processed in the following way (see Clementson's thesis [6]).[4] First, the signals from each of the 23 HgTe pixel elements used for the measurement were voltage-corrected to account for the slightly different thermal response of the heat absorbers. Second, the photon counts of these corrected voltage signals were co-added to form one data set for each electron-beam energy. Finally, the counts/voltage data sets were converted to a roughly linear photon energy scale by applying a calibration curve derived from known wavenumbers of the reference lines. Figure 2 of Clementson et al. [3] corresponds to the second step of this procedure, in which the voltage scale was replaced by an approximately linear energy scale. Therefore, it is easy to construct a secondary calibration curve from which the energies of each peak in the figure can be determined accurately. Figure 3 of the present paper shows the form of this secondary calibration curve, which is the dependence of the differences of the precisely measured energies of the peaks given in ref. 3 from the rough energies (inferred from the approximately linear energy scale of Fig. 2 of that paper) on photon energy.

Figure 3 shows that the energies of the peaks in Fig. 2 of [3] can be determined from the rough energy scale of that figure by applying a small correction of about 0.1% varying smoothly between 1 and 4 keV.

By analyzing the spectrograms given in the figures of Clementson et al. [3], several important observations can be made. First, there are some spectral lines not reported in that paper. Many of them belong to Cu-like W^{45+}. In particular, six lines between 1036 and 1351 eV (12 and 9.1 Å) were previously known with rather poor accuracy (±0.01 to ±0.016 Å) from the measurements of Ralchenko et al.

[4]Additional information was privately communicated to the author by J. Clementson. 2010.

[78] and Seely et al. [79] and from the isoelectronic interpolation of Seely et al. [80]. Clementson et al. [3] calibrated the energy scale of their spectrum using the line of Ni-like tungsten at 7.1733(3) Å [81] (shown by the blue circle in Fig. 3) and lines of H-like and He-like Na, Si, Cl, Ar, and K. In the present work, the calibration curve shown in Fig. 3 was built using the energies of tungsten lines listed by Clementson et al. [3] (including the Ni-like line at 7.1733 Å) and the Cu-like lines mentioned above. Using this calibration procedure, the wavelengths of these Cu-like lines can be determined much more precisely, as given in Table 2.

The second observation following from the analysis of Figs. 2–5 of Clementson et al. [3] is that this spectrum contains lines of Ga-like W^{43+}, Ge-like W^{42+}, and As-like W^{41+} not listed in ref. 3. In particular, in the interval 5.1–5.9 Å the strongest line of Ge-like W^{42+} reported by Neill et al. [76, 77] was at 5.8378 Å (see Kramida and Shirai [1]). In Fig. 2 of ref. 3, this line is not clearly resolved from the Ni-7 line at 5.8699 Å. However, it is distinctly resolved in Fig. 3 of the same paper depicting the spectrum acquired at the electron-beam energy of 3.3 keV. A weak line of Ge-like W^{42+} was reported by Neill et al. [76, 77] at 5.3457 Å with an intensity of 0.13 relative to the 5.8378 Å line. The line at 5.3435 Å was assigned by Clementson et al. [3] to Ni-like W^{46+} and labeled as Ni-9 in their Table 4. A peak at this wavelength is seen in their Figs. 2, 3, and 4 representing the spectra taken with the electron-beam energy of 4.0, 3.3, and 4.1 keV, respectively. Its intensity relative to the 5.8378 Å line as 0.37 and 0.23 at beam energies 4.0 and 3.3 keV, respectively. At the beam energy of 4.1 keV, the line of Ge-like W^{42+} at 5.8378 Å is not visible, while the peak at 5.3435 Å is present. Thus, the observed relative intensities justify the assignment of this peak to Ni-like W^{46+}. However, the Ge-like line at 5.3457 Å was observed by Neill et al. [76, 77] at much lower beam energies of 2.4 and 2.8 keV where the Ni-like spectrum was not excited. Therefore, their identification is also correct. A comparison of relative intensities of the Ni-9 line of Clementson et al. [3] at different electron-beam energies shows that at the lowest beam energy of 3.3 keV it is enhanced by about 30% due to blending with the Ge-like transition.

Pütterich et al. [14] have identified a line at 6.01(1) Å in a tokamak spectrum as a transition from the ground state to a $3d^94s^24p^24f$ ($J = 1$) level in Ge-like W^{42+}. This measured wavelength is somewhat lower than predicted by the parametric calculations [1], 6.042 Å. In the EBIT spectra of Clementson et al. [3] taken at beam energies of 3.3 and 4.0 keV, there is a distinct line at 6.0451(11) Å (not listed in their tables). The behavior of its intensity at different beam energies is similar to the lines of Ge-like W^{42+}, and both the wavelength and relative intensity agree with my calculations. Therefore, I identify it as the $3d^{10}4s^24p^2\ {}^3P_0$–$3d^9_{5/2}4s^2(4p^2({}^3P_0))(4f_{7/2})$ $(5/2, 7/2)^o_1$ transition in Ge-like W^{42+}. The wavelength disagrees with the measurement of Pütterich et al. [14]; however, they indicated that this line was blended in their experiment.

Clementson et al. [3] identified the line they observed at 5.7945(22) Å (denoted Zn-3 in their tables) as a two-electron transition in Zn-like W^{44+}. They noted that this line was previously observed by Neill et al. [76, 77] at 5.7928 Å and assigned to the Ga-like spectrum. The calculations made for the previous compilation [1] do not indicate any noticeable emission of Zn-like W^{44+} at this wavelength. On the other hand, the Ga-like line at this wavelength is the strongest one in the entire Ga-like spectrum between 4 and 10 Å (see the results of collisional-radiative modeling of Neu et al. [82]). Therefore, the line is undoubtedly due to Ga-like W^{43+}. A much weaker line of Ga-like W^{43+} was observed by Neill et al. [76, 77] at 5.302(3) Å. This line is very weak, but quite measurable in the spectra presented in Figs. 2 and 3 of Clementson et al. [3] taken at beam energies of 3.3 and 4.0 keV. The resulting average wavelength is 5.3013(8) Å. Three other Ga-like lines at 4.564(2), 4.047(2), and 3.964(2) Å were quoted in the previous compilation [1] from Tragin et al. [83]. These lines are also present in the spectra presented by Clementson et al. [3], and their wavelengths are 4.5608(6), 4.0472(12), and 3.9636(12) Å.

Pütterich et al. [14] have identified a line at 5.98(1) Å in a tokamak spectrum as a blend of transitions from the ground state $3d^{10}4s^24p\ {}^2P^o_{1/2}$ to $3d^94s^24p4f$ ($J = 1/2, 3/2$) levels in Ga-like W^{43+}. This line can be measured on the spectrograms presented by Clementson et al. [3]. Its wavelength, determined from the spectra taken at beam energies 3.3 and 4.0 keV, is 5.9996(11) Å. As follows from the parametric calculations performed for the previous compilation [1], the upper levels of two transitions responsible for this line are $3d^94s^24p(5/2, 1/2)^\circ_2 4f\ (2, 7/2)_{3/2}$ and $3d^94s^24p(5/2, 1/2)^\circ_3 4f\ (3, 7/2)_{1/2}$. Osborne et al. [8] have observed this line at 6.000 Å with an EBIT using the same microcalorimeter detector as in ref. 3 at electron-beam energies of 2.5–3.9 keV. Based on the behavior of its relative intensities at different beam energies, they tentatively assigned it to Ge-like W.

Clementson et al. [3] identified the line at 5.7450(4) Å, denoted Zn-4, as a blend of two transitions in Zn-like W^{44+}. They associated these transitions with the lines previously observed by Neill et al. [76, 77] at 5.7676 and 5.7471 Å. While the identification of the upper level responsible for the transition at 5.7471 Å agrees with the classification given in the previous compilation [1], Clementson et al. [3] suggested that the line at 5.7676 Å should be associated with a $(3d^9)_{5/2}4s_{1/2}4p_{3/2}4d_{5/2}$ level instead of $(3d^9)_{5/2}4s_{1/2}4p_{3/2}4d_{3/2}$. In this regard, it should be noted that there is one more line observed by Neill et al. [76, 77] at 5.7536 Å, which is midway between the two lines considered by Clementson et al. [3] to be components of the blend. The upper level of this line has almost equal contributions from the $4d_{3/2}$ and $4d_{5/2}$ states. It is probable that this is the same level that Clementson et al. [3] assigned to the 5.7676 Å line of Neill et al. [76, 77]. In the present work, the previous assignments of ref. 1 are retained.

Neu et al. [82] have identified the line at 7.410(15) Å that they observed in a tokamak spectrum as a blend of two transitions in As-like W^{41+} from the ground state $3d^{10}4s^24p^3\ {}^2D^o_{3/2}$ to the $3d^9_{5/2}4s^24p^4({}^3P_2)$ $(5/2, 2)_{3/2, 5/2}$ levels. This line was the strongest one in the spectrograms presented in their Figs. 1, 3*a*, and 3*b* covering the regions 6.3 to 10 Å, 7.0 to 8.4 Å, and 7.0 to 7.8 Å, respectively. This line is also distinctly seen in Fig. 8 of Pütterich et al. [14] showing the spectrum taken at the ASDEX Upgrade tokamak. It is the rightmost peak in the top panel of this figure, marked with a vertical arrow. This observation is especially interesting, because it corresponds to a much higher electron temperature of 3.9 keV (vs. 2.8 keV in Fig. 1 of Neu et al. [82]). At

such high electron temperatures the spectrum is dominated by strong lines of Ni-like W^{46+}. In the EBIT spectra of Clementson et al. [3], this line is distinctly seen at all electron-beam energies (3.3, 4.0, and 4.1 keV). It is located on the left of the peaks Zn-1 and Co-3 in Figs. 3 and 4 of ref. 3. Its wavelength, determined as a weighted mean of measurements at the three beam energies, is 7.4158(14) Å. It agrees well with the measurement of Osborne et al. [8] (7.411 Å), who unambiguously assigned this line to As-like W^{41+} based on the behavior of its intensity at electron-beam energies varying from 2.5 to 3.9 keV. Osborne et al. [8] corroborated this assignment by their collisional-radiative modeling. Another potentially strong line of As-like W^{41+} observed by Neill et al. [76, 77] at 5.8551 Å was apparently masked in the spectra of Clementson et al. [3] by the much stronger Ni-7 line. As observed by Osborne et al. [8] in the EBIT spectra at 2.5 and 2.7 keV, this line has about the same intensity as the 7.4158 Å line. At beam energies of 3.3–4.1 keV, used by Clementson et al. [3], its contribution to the Ni-7 line is negligibly small. The presence of the As-like line at 7.4158 Å in their spectrograms indicates that the lines of Ge-like and Ga-like ions should also be present, which supports identifications of these lines discussed above.

An important observation following from the analysis of wavelength measurements of Clementson et al. [3] concerns the narrow region between 2.1 and 2.5 keV (5.1–5.9 Å) previously investigated by Neill et al. [76, 77] using a high-resolution crystal spectrometer. In Fig. 3, the differences between the wavelengths measured by Neill et al. and those implied by the energy scale of Fig. 2 of Clementson et al. [3] are represented by the magenta squares. A clearly systematic behavior of these differences suggests that there was a problem with the wavelength calibration in the work of Neill et al. [76, 77].

Figure 4 quantifies this observation. In this figure, the differences between the energies of the peaks as measured by Neill et al. [76, 77] and those considered as reference values are plotted against the photon energy. For most of the data points, the reference values are those reported by Clementson et al. [3] in their tables. For a few data points for which the values were not given by Clementson et al. [3], I used the peak energies inferred from a detailed analysis of their Figs. 2, 3, and 4. The two data points at about 2.15 and 2.3 keV with very small error bars correspond to the two reference lines used by Neill et al. [76, 77]. These are the resonance lines of He-like ($1s^2\ {}^1S_0$–$1s2p\ {}^1P^o_1$) and H-like ($1s_{1/2}$–$2p_{3/2}$) phosphorus, for which Neill et al. used the wavelength values 5.7600 and 5.3814 Å without giving a reference. To my knowledge, the most precise published values for these lines are given by Johnson and Soff [84] and Drake [85]. These values (scaled according to the currently adopted values of the fundamental constants [70]) are 5.760 200 7(20) and 5.381 343 1(12) Å, respectively. The data points in Fig. 4 were fitted to a parabola by means of a weighted least-squares fitting procedure. Since the positions of the two phosphorus reference lines were measured by Neill et al. very precisely (with an uncertainty of ±0.0003 Å, or ±0.12 eV), this fitting procedure has only one effective degree of freedom, which is the curvature of the parabola. Thus, despite rather large uncertainties in the reference energies from Clementson et al. [3] (±0.6 eV on average), the large number of these reference points leads to a relatively small uncertainty in the calibration curve (smaller than ±0.2 eV for energies below 2370 eV, and increasing to ±0.5 eV at 2440 eV). The equation of the fitted parabola is

$$\Delta E = 563.327 - 0.504397E + 0.000112772E^2(\text{eV}) \qquad (2)$$

To correct the energies of the lines measured by Neill et al. [76, 77], their values must be decreased by the quantity ΔE given by this equation. This correction procedure affects all 64 wavelengths measured by Neill et al. [76, 77] in the spectra of Se-like W^{40+} through Cr-like W^{50+}. The magnitude of the correction is up to nine values of the total measurement uncertainties. The measurement uncertainties of Neill et al. must be combined in quadrature with the uncertainty of the calibration (given by the dotted lines in Fig. 4). The wavelengths of the lines from Neill et al., corrected as described above, are given in the data tables (see the online Supplementary Data) together with the increased uncertainty values.[2]

An important achievement of the work of Clementson et al. [3] is the first observation and identification of three lines arising from forbidden E2 transitions in Co-like W^{47+} at 7.3503(22), 7.667(5), and 7.7124(19) Å. These transitions may be useful for plasma diagnostics, since their intensities relative to allowed (E1) transitions depend on electron density.

One of the problems often encountered in articles interpreting complex atomic spectra is ambiguity of the energy level designations. For example, the two peaks of Cu-like W^{45+}, denoted Cu-3 and Cu-4 in Clementson et al. [3], have exactly the same designations of the lower and upper levels of the transitions, $3d^{10}4s_{1/2}$–$(3d^4_{3/2}3d^5_{5/2}4s_{1/2}4p_{3/2})_{1/2}$. The ambiguity arises from the omission of intermediate quantum numbers. In this particular case, the $4s_{1/2}$ and $4p_{3/2}$ electrons combined together give rise to two different states of the 4s4p subshell with $J = 1$ and $J = 2$. In the present data tables (see the online Supplementary Data) this ambiguity was resolved by means of a parametric fitting with Cowan's codes and finding the correct complete level designations and percentage compositions.[2]

2.5. Mn-like through Br-like (W XLIX–XL) [14]

The spectra of highly ionized tungsten in the regions 5–8 Å, around 50 Å, and between 100 and 300 Å were observed and analyzed by the ASDEX Upgrade Team [14]. Figure 8 of that paper presents the spectrum in the range 4–8 Å taken with a high-resolution crystal spectrometer. This spectrum contains about 130 lines having FWHM about 0.009 Å at 8 Å and 0.012 Å at 4 Å. Most of these lines can be identified with known transitions in Br-like W^{39+} through Mn-like W^{49+}. However, some of the moderately strong lines between 6.2 and 7 Å remain unidentified. The wavelengths of many strong lines in the region covered by this spectrum are now known with high precision. These known lines provide numerous references for internal calibration, enabling the wavelength measurement of the unknown lines with uncertainties as small as ±0.002 Å. Therefore, investigation of this spectrum should probably be revisited. Collisional-radiative modeling of this spectrum described in ref. 14 led to identification of new lines of Ga-like W^{43+}

and Ge-like W^{42+} described in Sect. 2.4 in connection with the work of Clementson et al. [3]. Previous identifications of many other lines have been confirmed.

The spectrum in the region 43–70 Å taken with a grazing-incidence spectrometer shows numerous superimposed peaks due to emission from I-like W^{28+} through Cu-like W^{46+}. This spectral feature has been successfully interpreted by Pütterich et al. [14] by means of collisional-radiative modeling. The previously-known wavelengths of strong isolated lines of these ions are of great help in such modeling.

The spectral region between 120 and 140 Å was found by Pütterich et al. [14] to be better suited for plasma diagnostics, because many of the spectral lines are well isolated. In this spectral region, they observed emissions of Se-like W^{40+} to Cu-like W^{45+}. Most of the line identifications given in Table 2 of their article agree with other work. There is a disagreement for the $4s^24p\ {}^2P^o_{3/2}$–$4s4p^2\ {}^2D_{5/2}$ transition in Ga-like W^{43+}. In ref. 14 following the work of Pütterich et al. [86], this transition was associated with the line at 135.34(5) Å. However, Ralchenko et al. [87] using EBIT spectra taken at different beam energies and isoelectronic comparisons have convincingly shown that this transition in Ga-like W^{43+} corresponds to a line they measured at 134.81(10) Å at beam energies lower than 2.2 keV. When the beam energy is gradually increased, this line becomes weaker and virtually disappears. When the beam energy is further increased, a strong line at 134.80(3) Å suddenly appears, simultaneously with other strong lines of Zn-like W^{44+}. Therefore, as given in Table 3 of Ralchenko et al. [87], the latter line corresponds to the M1 transition $4s4p\ {}^3P^o_1$–$4s4p\ {}^3P^o_2$ in Zn-like W^{44+}. As for the line at 135.34 Å, Ralchenko et al. [87] identified this line with the $4s^24p^2\ {}^3P_0$–$4s^24p^2\ {}^3P_1$ M1 transition in Ge-like W^{42+} and re-measured its wavelength to be 135.45(4) Å.

2.6. Pd-like W XXIX and UTA in In-like through I-like (W XXVI–XXII) [88]

The spectra of I-like through Pd-like W^{21+}–W^{28+} were observed by Chowdhuri et al. [88] in emission from the Large Helical Device (LHD) in Toki, Japan, by means of a flat-field holographic-grating spectrograph equipped with a charged-coupled-device detector. Although that work was published before the compilation [1] was completed, it was omitted in the compilation. In that experiment, tungsten was injected into the LHD plasma in the form of small carbon pellets containing thin tungsten wires. The spectrograph covered a large wavelength range from 20 to 500 Å. The spectral resolution was 0.16 Å at a wavelength of 70 Å. In addition to tungsten spectra, that work also included measurements of spectra of highly ionized molybdenum. Although the statistical uncertainties given in the tables of Chowdhuri et al. [88] are in the range 0.02–0.07 Å (as assessed from the variation of measured wavelengths in different exposures), the total measurement uncertainties are significantly greater. As follows from a comparison of the measured wavelengths from the more precise values given in the ASD database [89] and in the tables of ref. 88 for both molybdenum and tungsten spectra, the total uncertainties of the wavelengths measured by Chowdhuri et al. [88] are about ±0.15 Å in the wavelength range 48–85 Å. Apparently, they are dominated by calibration uncertainties.

In addition to several previously observed lines of W^{27+}–W^{29+}, Chowdhuri et al. reported a new identification of the $4d^{10}\ {}^1S_0$–$4d^95p\ {}^1P^o_1$ transition of Pd-like W^{28+} at 29.51 Å. This identification was based on extrapolation of observations available for lighter elements along the isoelectronic sequence made by Sugar and Kaufman [90].

For I-like through In-like W^{21+}–W^{28+}, Chowdhuri et al. reported the first measurement of wavelengths of the $4d^{10}4f^n$–$4d^{10}4f^{n-1}5g$ and $4d^{10}4f^n$–$4d^94f^n5p$ unresolved transition arrays (UTA) with $n = 3$–7. These wavelengths are in the range 30.9–38.1 Å. They are not included in the tables of the present paper because no level-specific information about the atomic structure can be extracted from them. Nevertheless, these observations may be important for plasma diagnostics.

These and other UTA spectra were further investigated, primarily theoretically, in the recent work of Harte et al. [91] with the main emphasis on the interpretation of experimental LHD spectra in the region 40–70 Å.

2.7. Tb-like through Hf-like (W X–III) [5, 92]

The spectra of Tm-like through Ho-like W^{5+}–W^{7+} in the region 180–450 Å were observed by Clementson et al. [5] in emission from a small spheromak device SSPX at LLNL equipped with a grazing-incidence spectrometer. Tungsten was injected into the plasma in the form of tungsten hexacarbonyl, $W(CO)_6$. The spectra showed a number of previously known lines of W^{5+} and W^{6+}. Besides that, there were numerous unknown lines tentatively assigned to W^{5+} through W^{7+}. The relatively low spectral resolution (about 0.3 Å) and blending by strong lines of O, C, and N did not allow precise identification of these unknown tungsten lines. However, two important conclusions follow from these observations. First, there are many unidentified lines in the spectra of Tm-like W^{5+} and Er-like W^{6+}, which show up in emission of the spheromak plasma (which is similar to that found in tokamaks). Therefore, despite the large number of already known lines of these spectra included in the previous compilation [1], these spectra need to be investigated more thoroughly. Second, the observed spectra definitely contain some lines of Ho-like W^{7+}. This spectrum was not analyzed before. Its presence in emission of plasmas similar to those of tokamaks necessitates a more thorough investigation. Such investigation is currently underway in collaboration between Observatoire de Paris-Meudon, Laboratoire Aimé Cotton, and the Institute of Spectroscopy of the Russian Academy of Sciences [92]. They obtained high-resolution (~0.015 Å) spectra of W VII–X from a triggered spark source in the region 150–350 Å with a grazing incidence spectrometer and even higher-resolution (~0.008 Å) spectra of W III–X from sliding spark and triggered spark sources in the region 500–1650 Å with a 10 m normal incidence spectrograph. The analysis of these extremely complex spectra has just started.

2.8. Hf-like and Ta-like (W III–II) [16, 15]

Nilsson et al. [16] and Palmeri et al. [15] measured radiative lifetimes in W II and W III using a time-resolved laser spectroscopy of a laser-produced plasma. They calculated the branching fractions using parametric calculations with Cowan's codes [93] modified to include the core-polarization potential. A combination of these calculated branching fractions with the measured lifetimes resulted in 290 new transition probability values in W II and several thousands in W III.

3. New theoretical interpretations of previously observed spectra

3.1 W I [17]

Wyart [17] made the first successful parametric interpretation of the odd-parity levels of neutral tungsten using the Hartree–Fock relativistic (HFR) method of Cowan [93]. In the analysis, he used a comparison of theoretical and experimental data on Landé factors and isotope shifts to verify the quality of the fitting procedure. As a result of this analysis, 215 energy levels of odd parity were fitted with a mean error of 131 cm^{-1}. Two new energy levels were found by classifying several previously unidentified spectral lines. This analysis enables a calculation of transition probabilities in W I. A few preliminary results compare well with existing experimental data. The improved theoretical description of this spectrum should make it possible to model this spectrum in fusion plasmas with much greater accuracy.

3.2 W XXX–XXXVIII [20] (Rh-like through Rb-like)

Jonauskas et al. [20] made an extensive theoretical re-examination of the spectra of M1 transitions within the $4p^64d^n$ ground configurations of Rh-like W^{29+} through Rb-like W^{37+}. These spectra were previously observed by Radtke et al. [94, 95] at the Berlin EBIT facility in the region 500–900 Å. The latter authors interpreted these spectra by collisional-radiative modeling using the Hebrew University Lawrence Livermore Atomic Code (HULLAC) [96]. Their calculations included only up to six interacting configurations for each ion, and the calculated wavelengths of M1 transitions deviated by up to 3% from the measured values. The line assignments relied to a large extent on the agreement of observed relative intensities of the lines with theoretical values.

Jonauskas et al. [20] used the FAC code by Gu [71] to calculate the energy levels, transition wavelengths, radiative rates, and collisional excitation cross sections. The calculated energy levels and wavelengths were cross-checked with the values calculated using the General Relativistic Atomic Structure Package (GRASP92) [97]. In the FAC calculations, the basis set was extended to 15–34 interacting configurations of even parity in addition to the ground configuration. The size of the basis set was limited by computer resources and was the smallest for Nb-like W^{33+} having the $4d^5$ ground configuration. Jonauskas et al. compared their calculated wavelengths and line intensities obtained with different sizes of basis sets, and concluded that they have achieved convergence of the calculations in terms of wavelengths, but not in terms of line intensities.

As a result of their work, Jonauskas et al. [20] have confirmed the previous identifications of 19 lines, suggested revised identifications of 14 lines, and questioned the previous identifications of 8 lines. While some of the suggested revisions seem to be reasonable, in many cases theoretically weak transitions are assigned to strong observed lines and vice versa, or a strong line is predicted at a wavelength near which there are no strong observed lines. For example, two strong lines observed at 706.18 and 708.22 Å with an intensity ratio of 3:1 [95] are assigned to transitions in Nb-like W^{33+} predicted at 705.73 and 704.49 Å. According to Fig. 2 of Jonauskas et al. [20], their collisional-radiative modeling predicts the ratio of intensities of these two lines to be 1:9. Furthermore, the argument of Jonauskas et al. [20] about the convergence of the calculated wavelengths is not very convincing. Their Fig. 4 illustrates the dependence of the calculated wavelength of the $(4d_{3/2})^3_{3/2}(4d_{5/2})^5_{5/2}$ $(J = 4)$–$(4d_{3/2})^4_0(4d_{5/2})^4_4$ $(J = 4)$ transition in Ru-like W^{30+} on the number of admixed configurations. When the number of configurations is between 4 and 15, the calculated wavelength is consistently close to the observed wavelength, 570.41(10) Å [95]. However, when more than 15 admixed configurations are included in the basis set, the calculated wavelength jumps upwards by about 2 Å and does not converge to the experimental value. In this case, the basis set could be extended to 28 admixed configurations. However, for most of the spectra calculated by Jonauskas et al. [20], limited computer resources did not allow them to include more than about 20 admixed configurations. Moreover, even if the calculations did converge, neither QED nor higher order effects were taken into account, and this may have introduced significant discrepancies from the actual wavelengths.

These considerations led me to a decision to leave the previous identifications of Radtke et al. [95] unchanged. However, the work of Jonauskas et al. [20] indicates that further theoretical analysis of the $4d^n$ spectra is needed and may result in significant revisions of line assignments.

3.3 W XIV [18, 19] (Pm-like)

Vilkas et al. [18] studied the spectra of Pm-like ions W^{13+} through U^{31+} by means of relativistic multireference Møller–Plesset second-order perturbation theory (MRMP). The most extensive results were obtained for Pm-like tungsten W^{13+}. By using a very large relativistic configuration interaction model, they claim to have achieved an accuracy of predicted wavelength about 0.25 Å for this ion in the region 240–420 Å. Their calculations have confirmed the previous assignment of the ground state of this ion to the $4f^{13}5s^2\,{}^2F^o_{7/2}$ level [1]. Much of the work is devoted to the search for the $4f^{14}5s\ {}^2S_{1/2}$–$4f^{14}5p\ {}^2P^o_{1/2,\,3/2}$ transitions. The calculations indicate that these transitions, occurring between excited states, are surrounded by numerous potentially stronger $4f^{13}5s^2$–$4f^{13}5s5p$ and $4f^{12}5s^25p$–$4f^{12}5s5p^2$ transitions. In Table 5 of their paper, Vilkas et al. [18] made a few tentative assignments for the lines observed previously in the Berlin EBIT spectra [98]. The latter paper gives two wavelengths, 365.3(2) and 258.2(2) Å, assigned to the $4f^{14}5s\ {}^2S_{1/2}$–$4f^{14}5p\ {}^2P^o_{1/2}$ and $4f^{14}5s\ {}^2S_{1/2}$–$4f^{14}5p\ {}^2P^o_{3/2}$ transitions, respectively. In that work, the spectra were recorded using a grazing-incidence spectrometer at electron beam energies that varied between 190 and 360 eV. The spectrograms presented in Fig. 1 of Hutton et al. [98] and Figs. 1 and 5 of Wu and Hutton [19] show that the line widths (FWHM) were 0.4–0.5 Å. Although the experimental wavelengths are given in Table 5 of Vilkas et al. [18] with two digits after the decimal point (e.g., 258.38 Å), they are quoted from a private communication from C. Biedermann and R. Hutton and originate in the same experimental study of Hutton et al. [98]. Therefore, they are likely to have the same uncertainties of about ±0.2 Å.

Wu and Hutton [19] discuss the behavior of relative intensities of the strong lines labeled as *a*, *b*, *c*, and *d* in their Fig. 5 at various electron-beam energies. The line *a*, which

Fig. 5. Dependence of ratios of normalized intensities of lines *a*, *c*, and *d* of Wu and Hutton [19] to the normalized intensity of line *b* on the electron beam energy. The error bars correspond to an uncertainty of 7%.

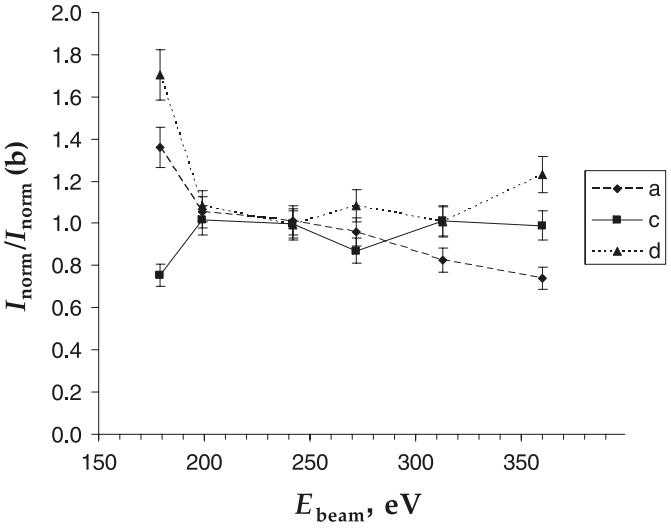

is the strongest one in the region 240–295 Å, corresponds to the wavelength 258.38 Å [18]. The lines *b* and *c* correspond to the wavelengths 261.10 and 272.05 Å, respectively. The line *d*, as inferred from Figs. 1 and 5 of Wu and Hutton [19], has a wavelength of 277.26(20) Å. Wu and Hutton [19], in their Fig. 2, plotted the dependences of the intensities of these four lines on the electron beam energy. Based on the similar shapes of these dependences they concluded that all four lines are likely to originate from the same ionization stage (presumably, Pm-like W^{13+}). A more informative comparison can be made by presenting the data plotted in that figure in a somewhat different way. Namely, for each of the lines let us call the ratio of intensity, *I*, to the maximum intensity, I_{max} (which is reached for all lines at the beam energy of 240 eV), a normalized intensity, I_{norm}. Then consider the ratios of the normalized intensities of lines *a*, *c*, and *d* to the normalized intensity of line *b*. The dependence of these ratios on the electron beam energy is plotted in Fig. 5.

As seen from Fig. 5, the ratio of normalized intensities of lines *c* and *b* is close to unity for all beam energies. This corroborates the conclusion of Vilkas et al. [18] that these lines can be attributed to the same ionization stage of tungsten. On the other hand, the ratio of lines *a* and *b* monotonically decreases with increasing beam energy. This, in agreement with Vilkas et al. [18], indicates that most of the intensity of line *a* is due to lower ionization stages. The ratio of lines *d* and *b* is close to unity at beam energies between 200 and 320 eV, but rises significantly at both lowest and highest beam energies. This indicates that the line *d* is a blend of both higher and lower ionization stages than those responsible for the line *b*.

Unfortunately, no such data on relative intensities are available for the lines at 253.84, 365.3, and 389.78 Å. It should be noted that the lines *b* (261.10 Å), *c* (272.05 Å), and 389.78 Å are assigned in ref. 18 to transitions from the ground state $4f^{13}5s^2\ {}^2F^o_{7/2}$ to some levels of the $4f^{13}5s5p$ configuration of Pm-like W^{13+}. Such electric-dipole transitions directly excited from the ground state are usually the strongest observed in EBITs. However, these particular transitions are by far not the strongest ones of this type predicted by the calculations of Vilkas et al. [18]. The transitions predicted at 244.795 and 245.055 Å have radiative rates about 200 times greater than the transitions assigned to the lines *a* and *b*. In Figs. 1 and 5 of Wu and Hutton, there is a relatively strong isolated line at about 242.9 Å. Its wavelength is 2 Å shorter than predicted by Vilkas et al. [18], and its intensity is about half of lines *b* and *c*. There are no other strong lines in its vicinity. This casts some doubt on the correctness of the identifications of ref. 18. However, it is well known that the transition rates alone do not describe the relative intensities in the EBIT spectra. Collisional-radiative modeling is necessary to confirm or disprove these identifications.

Another concern is the complete absence of the $4f^{11}5s^25p^2$ and $4f^{10}5s^25p^3$ configurations in the energy level table and the Grotrian diagram of Vilkas et al. [18]. According to my Cowan-code calculations, the $4f^{11}5s^25p^2$ configuration spreads between 192 000 cm^{-1} and 644 000 cm^{-1}, and its lowest levels are intermingled with the $4f^{12}5s^25p$ and $4f^{14}5p$ configurations. The $4f^{10}5s^25p^3$ configuration is located between 471 000 cm^{-1} and 1 037 000 cm^{-1}. Thus, the levels $4f^{14}5p\ {}^2P^o_{3/2}$ and $4f^{14}5p\ {}^2P^o_{1/2}$ (predicted at 564 166 cm^{-1} and 449 903 cm^{-1}, respectively, [18]) should have sequential numbers 95 and 30 among levels with $J = 3/2$ and 1/2, respectively, instead of 12 and 8 specified in Table 5 of Vilkas et al. [18]. If the configurations $4f^{11}5s^25p^2$ and $4f^{10}5s^25p^3$ were not included in the calculations of Vilkas et al. [18], it could affect the calculated energies of odd-parity levels. Although the parameters corresponding to the first-order perturbations caused by interactions between these configurations and $4f^{14}5p$ are exactly zero, the higher-order perturbations can be significant in a calculation aiming at spectroscopic accuracy.

4. Purely theoretical studies

4.1. RMBPT calculations

Safronova et al. [26] employed the relativistic many-body perturbation theory (RMBPT) to calculate the energy levels and radiative and autoionization rates for the $1s2l2l'$ states of Li-like W^{71+} and several other isoelectronic ions. These data may be useful for diagnostics of high-temperature core plasmas of the future fusion reactors in the X-ray region around 0.2 Å. Safronova et al. [26] also calculated the energies of the $2s_{1/2}$–$2p_{3/2}$ transitions in Li-, Be-, and B-like W, Th, and U. Their results for tungsten are in agreement with the recent measurements of Podpaly et al. [10] and Clementson et al. [7], except for Li-like W^{71+}, for which the calculated energy is 0.8(5) eV higher than the experimental one [7]. This deviation follows the same trend as for Th and U, for which the deviations are 0.88(14) and 1.56(25) eV, respectively.

Safronova and Safronova [27] used the RMBPT method to calculate energy levels and radiative rates of W^{70+}, W^{69+}, W^{62+}, W^{61+}, W^{54+}, W^{44+}, W^{27+}, and W^{4+} (Be-, B-, Mg-, Al-, Ca-, Zn-, Ag-, and Yb-like). For Be-like W^{70+}, the energies of $1s^22l2l'$ and $1s^22l3l'$ and E1 transition rates for the $\Delta n = 0$, 1 transitions were calculated. The energies of the $1s^22s2p$ levels were previously calculated by Cheng et al. [34] (using a relativistic configuration-interaction (RCI) method) and by Safronova et al. [99] (using RMBPT with

a different approximation for the QED effects). All these theories agree with each other and with the only available measurements of the $1s^2 2s2p\ {}^1P_1^o$ level [10, 7] within 8000 cm^{-1}. For the $1s^2 2p^2$ levels, the excitation energies calculated by Safronova and Safronova [27] are lower than those calculated by Safronova et al. [99] by approximately 15 000 cm^{-1}.

For B-like W^{69+}, the excitation energies given by Safronova and Safronova [27] are the same (within rounding errors) as those calculated by Safronova et al. [100]. However, the labels of the two even-parity levels with $J = 1/2$ at 14 251 000 and 26 161 200 cm^{-1} appear to be incorrectly interchanged in [27] (in both the *jj* and *LS* coupling schemes). Similarly, the labels of the two odd-parity levels with $J = 3/2$ at 16 532 780 and 27 931 920 cm^{-1} are interchanged. The *jj*-coupling labels were given correctly in [100]. The calculated energies of the $2s_{1/2}(2p_{1/2}2p_{3/2})_1\ (1/2,\ 1)_{1/2,\ 3/2}$ and $2s_{1/2}(2p_{1/2}2p_{3/2})_2\ (1/2,\ 2)_{3/2}$ levels and $2s2p^2\ (1/2,\ 0)_{1/2}$–$2s^2 2p_{3/2}$ interval agree with the measurements of Podpaly et al. [10] and Clementson et al. [7] with an average deviation of 2800 cm^{-1}. Designations and percentage compositions of these levels in the *LS* coupling scheme (see the online Supplementary Data) were found in the present work using Cowan-code calculations.[2] In addition to the energies, Safronova and Safronova [27] calculated the radiative rates of the $\Delta n = 0$ E1 transitions between the $n = 2$ levels of B-like W^{69+}.

For Mg-like W^{62+}, Safronova and Safronova [27] calculated the excitation energies of the $[2p^6]3s^2$, 3s3p, $3p^2$, 3s3d, 3p3d, and $3d^2$ levels and radiative rates of the E1 transitions between them. The experimental energies of the three known excited levels ($3s3p\ {}^{1,3}P_1^o$ and $3s3d\ {}^3D_2$) derived from the wavelengths measured by Ralchenko et al. [75] and by Clementson and Beiersdorfer [2] agree with the calculations of Safronova and Safronova [27] within 4000 cm^{-1}.

For Al-like W^{61+}, Safronova and Safronova [27] calculated the excitation energies of the $[2p^6]3s^2 3p$, $3s3p^2$, $3d^2 3d$, 3s3p3d, and $3p^3$ levels and radiative rates of the E1 transitions between them. The experimental energies of the six known levels derived from the wavelengths measured by Ralchenko et al. [75] and by Clementson and Beiersdorfer [2] agree with the calculations of Safronova and Safronova [27] within 2900 cm^{-1}. However, the designations of several levels given by Safronova and Safronova [27] appear to be incorrect. For example, the level at 4 815 010 cm^{-1} is designated $3s(3p_{3/2}3p_{3/2})_2\ (1/2,\ 2)_{3/2}$ (or $3s3p^2\ {}^2P_{3/2}$ in the *LS* coupling). It corresponds to the experimental level at 4 817 900(900) cm^{-1} derived from the strongest observed transition of Al-like W^{61+} at 20.756(4) Å [2] and identified as $3s^2 3d\ {}^2D_{3/2}$. The level at 5 405 950 cm^{-1}, designated $3s(3p_{3/2}3p_{3/2})_2\ (1/2,\ 2)_{5/2}$ (or $3s3p^2\ {}^2D_{5/2}$), according to my parametric calculations with Cowan's codes must be designated $3s^2 3d\ {}^2D_{5/2}$. The levels at 7 063 900, 7 365 100, and 7 405 190 cm^{-1}, denoted in the *LS* coupling $3s^2 3d\ {}^2D_{5/2}$, $3s3p^2\ {}^2P_{1/2}$, and $3s^2 3d\ {}^2D_{3/2}$ [27], must be designated $3s3p^2\ {}^4P_{5/2}$, ${}^2S_{1/2}$, and ${}^2P_{3/2}$. The level at 4 182 210 cm^{-1}, denoted $3s3p^2\ {}^4P_{5/2}$ [27], must be designated $3s3p^2\ {}^2D_{5/2}$.

For Ca-like W^{54+}, Safronova and Safronova [27] calculated the energy levels of the ground configuration $3s^2 3p^6 3d^2$ and radiative rates of M1 and E2 transitions between them. Their calculated energy levels agree with the FAC calculations of Reader et al. [9] within 2700 cm^{-1}. A similar agreement exists between the calculated energies and experimental values derived from the observed wavelengths of M1 transitions [9]. The *LS* designations of the highly mixed $^3P_2$ and $^1D_2$ levels may have been interchanged.

For Zn-like W^{44+}, Safronova and Safronova [27] calculated the energy levels of the $[3d^{10}]4s^2$, 4s4p, 4s4d, 4s4f, $4p^2$, 4p4d, 4p4f, 4d4f, $4d^2$, and $4f^2$ configurations and radiative rates of E1 transitions between them. The calculated energies of the 4s4p levels agree with the experimental data [1] within 11 000 cm^{-1}. At first glance, there appears to be a gross disagreement (by up to 450 000 cm^{-1}) with the known 4s4d levels with $J = 2$. However, examination of the complete level list given in Table 1 of [27] shows that the problem is the same as in the Al-like spectrum. Namely, the designations of several levels with the same J value are interchanged in ref. 27. The identity of the levels can easily be established with the help of Cowan-code calculations, taking into account that the energy ordering of levels with the same J is actually the same in the Cowan-code and RMBPT calculations for this particular spectrum. Thus, the level designated in ref. 27 $4s_{1/2}4d_{3/2}$ ($J = 2$, energy 2 359 810 cm^{-1}) is actually $4p^2\ {}^1D_2$; the level designated $4s_{1/2}4d_{5/2}$ ($J = 2$, energy 2 809 010 cm^{-1}) is actually 4s4d $^3D_2$ (or 4s4d $(1/2,\ 3/2)_2$ in the *jj*-coupling scheme), and the level designated $4p_{1/2}4p_{3/2}$ ($J = 2$, energy 2 997 790 cm^{-1}) is actually 4s4d $^1D_2$ (or 4s4d $(1/2,\ 5/2)_2$ in *jj*-coupling). Then it turns out that the 4s4d energies calculated in ref. 27 actually agree with the experimental ones given in ref. 1 within 9000 cm^{-1}.

For Ag-like W^{27+}, Safronova and Safronova [27] calculated the energy levels of the $4d^{10}4f$, 5s, 5p, 5d, 5f, and 5g configurations and radiative rates of E1 transitions between them. The fine-structure splitting of the ground configuration $4d^{10}4f$ agrees with the experimental value given in ref. 1 within 3500 cm^{-1}.

For Yb-like W^{4+}, Safronova and Safronova [27] were the first to make an ab initio calculation of the 5d*nl* (*nl* = 5d, 6s, and 6p) energy levels and radiative rates of E1 transitions between them, as well as the energy levels of the 5d5f, $6s^2$, and 6s6p configurations. The calculated energies are compared with the NIST values from [1] in Table 17 of ref. 27. Good agreement was found (the root-of-mean-square relative deviation is 2.6% for $5d^2$ and 1.2% for the rest of the levels).

Another work of Safronova and Safronova [28] gives results of RMBPT calculations of energy levels and radiative rates in Zn-like ions from $Z = 32$ to 100. They compare their calculated wavelengths with experimental data for the $4s^2$–4s4p, 4s4p–4s4d, and 4s4p–$4p^2$ transitions in the interval $Z = 70$–92. This comparison was largely based on experimental wavelengths from the work of Brown et al. [101] where the Zn-like spectra of several elements with $Z = 50$–92 were investigated. The spectra were produced by irradiating thick planar targets using one beam of the Nova laser at LLNL. Line identifications were based on isoelectronic comparisons and on comparisons with multiconfiguration Dirac–Fock (MCDF) calculations. The results of that work were not included in the compilation [1] for two reasons. First, the accuracy of measurements made with such laser-produced plasmas was doubtful, because similar studies in copper-like spectra, made with the same laser, suffered from large systematic shifts. Second, the isoelectronic comparisons with

theory in many cases were inconclusive because of avoided level crossings in the vicinity of $Z = 70$. Such level crossings result in large deviations of experimental wavelengths from theoretical wavelengths, which are not smooth along the sequence. However, the complete omission of the work of Brown et al. [101] in the compilation [1] was a mistake. Now, the good agreement between the RMBPT calculations of Safronova and Safronova [27, 28], MRMP calculations of Vilkas and Ishikawa [102], semiempirical results of Brown et al. [101], and several firmly established experimental values of energy levels [1] makes it possible to confirm the accuracy of the measurements of Brown et al. [101], and confirm several of their line identifications. Some of their identifications must be rejected because they contradict more precise measurements adopted in [1]. Namely, the two lines at 73.840(20) and 76.516(20) Å were assigned by Brown et al. [101] to the 4s4p $(1/2, 3/2)^{o}_{1}$–4s4d $(1/2,5/2)_2$ and 4s4p $(1/2,3/2)^{o}_{2}$–4s4d $(1/2,3/2)_2$. These wavelengths deviate from the Ritz values by +0.4 and –0.5 Å, respectively. Calculations of line intensities in the model with Boltzmann populations of levels result in very small predicted intensities of these lines. In the present Tables (see the online Supplementary Data), only the lines predicted to have reasonably large intensities are included from [101]. These lines establish three energy levels of the $4p^2$ configuration and one level in each of the 4s4d and 4p4d configurations.[2]

Safronova and Safronova [29] calculated the excitation energies and E1 transition rates of several Ag-like ions, including W^{27+}. The calculated wavelengths of several lines around 50 Å agree with the observations [1] within 0.5 Å. Similar agreement with experimental data is found for Yb^{23+} and Er^{21+}.

Safronova et al. [30, 31] made extensive calculations of energy levels, radiative and autoionization rates, dielectronic satellite lines and dielectronic recombination rates for Mg-like W^{62+} and Na-like W^{63+}. They employed RMBPT, HULLAC, and Cowan atomic codes and compared the results obtained with them. These calculations may help to interpret the complex spectra in the vicinity of the resonance lines of Ne-like W^{64+} between 1.18 and 1.56 Å observed by the Berlin EBIT team [12, 13].

Safronova et al. [32] calculated radiative transition rates for E2, M1, and M3 transitions between the levels of the $3d^{10}$, $3d^9$4s, 4p, and 4d configurations of several Ni-like ions including W^{46+} using RMBPT. Although the important E2 and M3 $3d^{10}$–$3d^9$4s transitions near 7.9 Å are not included in the tables of that article, their rates can be inferred from the graphs given in the figures.

Blundell et al. [42] made RMBPT calculations of the energies of the $n = 4$ states along the Zn isoelectronic sequence ($Z = 30$–100). For W^{44+}, the only numerical result given in the tables of that article is for the $4s^2\ {}^1S_0$–4s4p $^1P^{o}_1$ transition. It agrees with the experimental value within 630 cm^{-1}. Intervals between several levels of the 4s4p, 4p4d, 4s4f, 4d4f, $4p^2$, 4s4d, $4d^2$, and 4p4f configurations can be inferred from plots of isoelectronic dependences given in the figures.

Blundell [41] made impressively precise calculations of the QED corrections to the RMBPT energy of the $4s^2\ {}^1S_0$–4s4p $^1P^{o}_1$ transition in Zn-like ions ($Z = 70$–92). His results, combined with RMBPT calculations of Blundell et al. [42], agree with all available experimental data within one or two experimental standard-deviation uncertainties. In particular, for W^{44+} his result differs from experiment by only 134 cm^{-1}, while the experimental uncertainty is 140 cm^{-1}.

4.2. MRMP calculations

Vilkas et al. [45] employed the relativistic multireference Møller-Plesset second-order perturbation theory (MRMP) to calculate the energy levels and transition probabilities in Ne-like Xe^{44+}, W^{64+}, and U^{82+}. Their calculated energy levels of W^{64+} agree with the available experimental data [1] remarkably well. The root-of-mean-square deviation of the calculated values from the four available experimental values (the $2s2p^63p\ (1/2,1/2)^{o}_{1}$ and $2s^22p^5(^2P^{o}_{1/2})3d\ (1/2,3/2)^{o}_{1}$ levels [1] and the intervals between the $2s^22p^5(^2P^{o}_{3/2})3s\ (3/2,1/2)^{o}_{1}$ and the $2s^22p^5(^2P^{o}_{3/2})3p\ (3/2,3/2)^{o}_{0}$ and $2s^22p^5(^2P^{o}_{1/2})3p\ (1/2,1/2)^{o}_{0}$ levels [2, 7]) is only 0.02%.

4.3. Calculations of hyperfine-induced forbidden transitions

A review of experiments and theory on the hyperfine-induced transitions in neutral and ionized atoms was given by Johnson [103]. These transitions were also discussed by Hutton et al. [104] (see also references therein). One of the types of atomic systems where such transitions occur is Ni-like ions. In these ions, the $F = 5/2$ sublevel of the $3d^94s\ {}^3D_3$ level is quenched by mixing with the $^{1,3}D_2$ states induced by hyperfine interactions. In Ni-like W^{46+}, this level is responsible for the important density-dependent M3 transition at 7.9374(7) Å [4]. Tungsten has only one stable isotope having nonzero nuclear moment, ^{183}W. Its abundance in the composition of natural tungsten is 14.28% [105], and its nuclear moment is relatively small. Therefore, the hyperfine quenching can make only a very small contribution to the decay rate. Nevertheless, a calculation of the hyperfine-induced rate for $^{183}W^{46+}$ may be of interest at least from the point of view of estimating the size of this contribution.

Cheng et al. [34] investigated the hyperfine quenching of the $2s2p\ {}^3P^{o}_0$ state of Be-like ions ($Z = 6$–92) using the RCI method. They made a high-precision calculation of the excitation energies of the $2s2p\ {}^{1,3}P^{\circ}$ levels of Be-like ions. For tungsten their calculated energies are higher than those calculated by Safronova and Safronova [27] by 7500 cm^{-1} on average. This average deviation can be adopted as an estimate of uncertainty. Then the $2s^2\ {}^1S_0$–$2s2p\ {}^3P_0$ forbidden transition is predicted to occur at 72.1(4) Å in W^{70+}. The calculated rate of the hyperfine-induced $2s^2\ {}^1S_0$–$2s2p\ {}^3P_0$ transition in ^{183}W is 1326 s^{-1} [34].

Kang et al. [36] calculated the radiative rates of the hyperfine-induced forbidden transition $3s^2\ {}^1S_0$–$3s3p\ {}^3P^{\circ}_0$ transition in Mg-like ions ($Z = 12$–80) using the MCDF method. Although they did not give a numerical value for $^{183}W^{62+}$, it can be inferred from the isoelectronic plot given in their Fig. 2.

Hyperfine-induced transitions may occur in many other atomic systems, e.g., Ti-like, Zn-like, and Ne-like [103]. They may also be important for collisional-radiative modeling of hot plasmas.

4.4. Other theoretical studies

Kučas et al. [21] explored the effects of interactions be-

tween the $4p^5 4d^{n+1}$ and $4p^6 4d^{n-1} 4f$ configurations along isoelectronic sequences of Sr through Ru and along the isonuclear sequence of W^{29+} through W^{37+} ions having the ground configurations $4p^6 4d^n$ (n = 1–10). This study explains the mechanism of formation of compact groups of strong lines in these spectra.

Karpuškienė et al. [24] made an ab initio calculation of transition probabilities of singly ionized tungsten (W II) using a new quasirelativistic multiconfiguration method (see references in [24]). Although it is doubtful that these calculations can compete in accuracy with the semiempirical calculations of Nilsson et al. [16], they revealed an important fact. Namely, these calculations extend to shorter wavelengths (down to 1000 Å), compared to experimental data [1] (1528–5708 Å), and reveal the presence of numerous previously unobserved strong lines below 1500 Å.

Gaigalas et al. [25] studied the properties of Sn-like W^{24+} using ab initio MCDF calculations. This spectrum is peculiar because its ground configuration $4d^{10}4f^4$ does not combine with the first excited configuration $4d^{10}4f^3 5s$ via single-electron electric-dipole transitions because of the selection rules for such transitions. Therefore, the $4d^{10}4f^3 5s$ configuration is metastable and can accumulate a significant population. This makes it possible to observe the $4d^{10}4f^3 5s$–$4d^{10}4f^3 5p$ electric-dipole transitions predicted to occur in two compact groups in the regions 170–200 and 290–310 Å.

Quinet et al. [22] critically evaluated the existing experimental and theoretical data on transition probabilities of electric-dipole transitions and calculated transition rates of forbidden (M1 and E2) transitions in W I–III. They presented data for selected lines of these spectra suitable for plasma diagnostics and modeling of fusion reactors.

Biémont et al. [23] presented theoretical Landé factors of W II and W III calculated using the parametric semiempirical models developed by Nilsson et al. [16] and Palmeri et al. [15]. The calculated values are in good agreement with available experimental data [1], but cover much larger sets of energy levels.

Chen and Cheng [33] calculated the excitation energies of the 4s4p levels in Zn-like ions (Z = 30–92) and radiative rates of the resonance and intercombination transitions using the RCI method with QED corrections. Their calculated energies are in good agreement with the RMBPT calculations of Safronova and Safronova [27, 28] and with other high-precision calculations discussed above. The calculated rates provide another set of data for comparison with other calculations and will help to evaluate the accuracy of calculations.

Li et al. [35] calculated the radiative rates of two-electron–one-photon M1 and E2 transitions between the states of the $2p^3$ and $2s^2 2p$ configurations of B-like ions (Z = 18–92), including W^{69+}, using the MCDF method. Their results may be useful in collisional-radiative modeling of hot plasmas.

Xie et al. [37] calculated the radiative rates of two-electron one-photon transitions in highly charged Ni-like ions (Z = 47–92). The results are given in the form of isoelectronic plots from which the data for Ni-like W^{46+} can be inferred.

Li et al. [38] calculated the excitation energy of the $2s2p^4$ $(^3P_2)$ $(1/2, 2)_{5/2}$ level of N-like ions (Z = 50–92) using the MCDF method. They measured the energy of the transition from this level to the ground state in $^{208}Pb^{75+}$ at the Tokyo EBIT facility. Experimental data on this level exist for Z = 90 and 92. The recent measurements of Podpaly et al. [10] and Clementson et al. [7] for W^{67+} provide another point for isoelectronic comparison. Calculations of Li et al. [38] agree with all experiments within a fraction of an eV.

Ivanova [39] calculated excitation energies of the $4d^{10}4f$, $5l$ (l = 0–3) levels in Ag-like ions, $4d^9 4f$, 5p, and 5f (J = 1) levels in Pd-like ions, and $4d^9$ levels in Rh-like ions (Z = 52–86) using the relativistic perturbation theory model potential method (RPTMP). She also calculated the ionization energies of these ions. Her results may be useful in analyzing isoelectronic trends. Using the same RPTMP method, Ivanova [40] calculated radiative rates of E1 transitions (5s–5p, 5p–5d, 5d–5f, and 4f–5d) in Ag-like ions (Z = 50–86).

Puchkov and Labzovskiĭ [43] studied the forbidden M1 transitions in hydrogen-like spectra. They derived explicit formulas for the probabilities of these transitions, showing the strong (Z^{10}) dependence on the nuclear charge. The potential application to tungsten, although rather fantastic at present, involves the possibility that the $1s_{1/2}$–$2s_{1/2}$ transition of W^{73+} at 0.206 169 5(21) Å [1] may be strong enough to be observable. Of course, it would be very difficult to resolve it from the $1s_{1/2}$–$2p_{1/2}$ transition at 0.206 252 8(21) Å [1]. However, if such a measurement were accomplished, it would be useful as a direct test of the QED theory for heavy ions.

Wang et al. [44] investigated effects of electron correlations and Breit interactions on the fine structure of ground configurations of N-like ions (Z = 8–100) using the MCDF method. Their findings may be of interest for theorists.

Rhee and Kwon [48] employed the MCDF method to calculate the transition probabilities of tungsten ions from W^{33+} to W^{37+} (Nb-like through Rb-like) for transitions between the $4p^6 4d^n$ and $4p^5 4d^{n-1} + 4p^6 4d^{n-1} 4f$ configurations in the range of 40–75 Å.

Desclaux [49] applied the MCDF method to the calculation of the radiative decay rates from the lowest J = 7/2 level of the $4s^2 4p^4 4d$ configuration along the bromine isoelectronic sequence. This level is metastable and can decay to the ground configuration $4s^2 4p^5\ ^2P^\circ$ only via weak M2 and E3 transitions. It can also decay to lower levels of the $[4s^2 4p^4]$ 5s and 4d configurations via M1 and E2 transitions. One of such transitions in Br-like W^{39+} (at 698.4 Å) was identified by Radtke et al. [95] in the spectrum observed with the Berlin EBIT. The rates of various decay channels can be inferred from isoelectronic plots given by Desclaux [49].

Mandelbaum and Schwob [46] calculated the energy levels, ionization energies, and electron-impact ionization cross-sections for Ga-like ions (Z = 36–92) using the HULLAC computer package. In terms of the energy structure, their results may be useful in analyzing isoelectronic trends.

Charro et al. [50] calculated radiative rates of forbidden (M1 and E2) $4p_{1/2}$–$4p_{3/2}$ transitions within the ground configuration $3d^{10}4s^2 4p$ in Ga-like ions (Z = 31–80). They used the relativistic quantum defect orbital (RQDO) method.

Feldman et al. [47] investigated the possible use of spectral lines from highly ionized tungsten in measuring radiation transport and other physical properties of ITER plasmas. They gave a list of theoretical wavelengths (calculated by means of the FAC code [71]) of bright lines in W^{58+} through W^{71+} (S-like through Li-like) that are predicted to be useful for diagnostics of hot plasma of the tokamak core. They cal-

Table 3. Index to recent publications on tungsten spectra.

Spectrum	Ion charge	Sequence	Ref.	Subject of work	Sections in text
W I	0	W	[17]	EL, CL, ZE, PT, TP	3.1
			[22]	TP	4.4
W II	1	Ta	[23]	ZE, SE, PT	4.4
			[22]	TP	4.4
			[16]	TP	2.8, 4.4
			[24]	TP	4.4
W III	2	Hf	[23]	ZE, SE, PT	4.4
			[22]	TP	4.4
			[15]	PT, TP	2.8, 4.4
W V	4	Yb	[27]	TE, AT, TP	4.1, 4.3, 4.4
W VI	5	Tm	[5]	W	2.7
W VII	6	Er	[5]	W	2.7
W VIII	7	Ho	[5]	W	2.7
W XIV	13	Pm	[19]	CL	3.3
			[18]	CL, W, TE, AT, TP	3.3
W XV	14	Nd	[91]	TA	2.6
W XVI	15	Pr	[91]	TA	2.6
W XVII	16	Ce	[91]	TA	2.6
W XVIII	17	La	[91]	TA	2.6
W XIX	18	Ba	[91]	TA	2.6
W XX	19	Cs	[91]	TA	2.6
W XXI	20	Xe	[91]	TA	2.6
W XXII	21	I	[91]	TA	2.6
			[88]	TA	2.6
W XXIII	22	Te	[91]	TA	2.6
			[88]	TA	2.6
W XXIV	23	Sb	[91]	TA	2.6
			[88]	TA	2.6
W XXV	24	Sn	[25]	TE, AT, TP	4.4
			[91]	TA	2.6
			[88]	TA	2.6
W XXVI	25	In	[91]	TA	2.6
			[88]	TA	2.6
W XXVII	26	Cd	[91]	TA	2.6
W XXVIII	27	Ag	[27]	TE, AT, TP	4.1, 4.3, 4.4
			[29]	TE, AT, TP	4.1
			[39]	TE, IP, PT	4.4
			[91]	TA	2.6
			[40]	TP	4.4
W XXIX	28	Pd	[88]	CL, W	2.6
			[91]	TA	2.6
			[39]	TE, IP, PT	4.4
W XXX	29	Rh	[39]	TE, PT	4.4
			[91]	TA	2.6
			[20]	CL, TE, AT, TP	3.2
			[21]	AT	4.4
W XXXI	30	Ru	[20]	CL, TE, AT, TP	3.2
			[92]	TA	2.6
			[21]	AT	4.4
W XXXII	31	Tc	[20]	CL, TE, AT, TP	3.2
			[91]	TA	2.6
			[21]	AT	4.4
W XXXIII	32	Mo	[20]	CL, TE, AT, TP	3.2
			[91]	TA	2.6
			[21]	AT	4.4
W XXXIV	33	Nb	[20]	CL, TE, AT, TP	3.2
			[91]	TA	2.6

Table 3 (*continued*).

Spectrum	Ion charge	Sequence	Ref.	Subject of work	Sections in text
			[21]	AT	4.4
			[48]	TP	4.4
W XXXV	34	Zr	[20]	CL, TE, AT, TP	3.2
			[91]	TA	2.6
			[21]	AT	4.4
			[48]	TP	4.4
W XXXVI	35	Y	[20]	CL, TE, AT, TP	3.2
			[91]	TA	2.6
			[21]	AT	4.4
			[48]	TP	4.4
W XXXVII	36	Sr	[20]	CL, TE, AT, TP	3.2
			[91]	TA	2.6
			[21]	AT	4.4
			[48]	TP	4.4
W XXXVIII	37	Rb	[20]	CL, TE, AT, TP	3.2
			[91]	TA	2.6
			[21]	AT	4.4
			[48]	TP	4.4
W XL	39	Br	[14]	CL, W	2.4, 2.5
			[49]	TP	4.4
W XLI	40	Se	[14]	CL, W	2.4, 2.5
W XLII	41	As	[3]	W	2.4, 2.5
			[8]	CL,W	2.4
			[14]	CL, W	2.4, 2.5
W XLIII	42	Ge	[3]	W	2.4, 2.5
			[8]	CL,W	2.4
			[14]	CL, W	2.4, 2.5
W XLIV	43	Ga	[3]	W	2.4, 2.5
			[8]	CL,W	2.4
			[14]	CL, W	2.4, 2.5
			[46]	TE, IP, AT	4.4
			[50]	TP	4.4
W XLV	44	Zn	[3]	CL, W	2.4, 2.5
			[8]	CL,W	2.4
			[14]	CL, W	2.4, 2.5
			[101]	CL, W, TE	4.1
			[27]	TE, AT, TP	4.1, 4.3, 4.4
			[28]	TE, SE, AT, TP	4.1, 4.4
			[33]	TE, AT, TP	4.4
			[41]	TE, AT	4.1
			[42]	TE, AT	4.1
W XLVI	45	Cu	[3]	CL, W	2.4, 2.5
			[8]	CL,W	2.4
			[14]	CL, W	2.4, 2.5
			[12]	W	4.1
			[42]	TE, AT	4.1
W XLVII	46	Ni	[3]	CL, W	2.4, 2.5
			[8]	CL,W	2.4
			[4]	CL, W	2.4, 4.3
			[14]	CL, W	2.4, 2.5
			[12]	W	4.1
			[37]	TE, AT, TP	4.4
			[32]	TP	4.1
W XLVIII	47	Co	[3]	CL, W	2.4, 2.5
			[9]	CL, W	2.3, 4.1
			[14]	CL, W	2.4, 2.5
			[12]	W	4.1

Table 3 (*continued*).

Spectrum	Ion charge	Sequence	Ref.	Subject of work	Sections in text
W XLIX	48	Fe	[9]	CL, W	2.3, 4.1
			[14]	CL, W	2.4, 2.5
			[12]	W	4.1
W L	49	Mn	[9]	CL, W	2.3, 4.1
			[12]	W	4.1
W LI	50	Cr	[9]	CL, W	2.3, 4.1
			[12]	W	4.1
W LII	51	V	[9]	CL, W	2.3, 4.1
W LIII	52	Ti	[9]	CL, W	2.3, 4.1
W LIV	53	Sc	[9]	CL, W	2.3, 4.1
W LV	54	Ca	[9]	CL, W	2.3, 4.1
			[27]	TE, AT, TP	4.1, 4.3, 4.4
W LVI	55	K	[2]	CL, W	2.2, 4.1, 4.2
			[9]	CL, W	2.3, 4.1
W LVII	56	Ar	[2]	CL, W	2.2, 4.1, 4.2
W LVIII	57	Cl	[2]	CL, W	2.2, 4.1, 4.2
			[14]	TE	2.4, 2.5
W LIX	58	S	[2]	CL, W	2.2, 4.1, 4.2
			[14]	TE	2.4, 2.5
			[47]	TE, AT	4.4
W LX	59	P	[2]	CL, W	2.2, 4.1, 4.2
			[14]	TE	2.4, 2.5
			[47]	TE, AT	4.4
W LXI	60	Si	[2]	CL, W	2.2, 4.1, 4.2
			[11]	CL, W	2.1, 2.2
			[13]	W	4.1
			[12]	W	4.1
			[14]	TE	2.4, 2.5
			[47]	TE, AT	4.4
W LXII	61	Al	[2]	CL, W	2.2, 4.1, 4.2
			[11]	CL, W	2.1, 2.2
			[13]	W	4.1
			[12]	W	4.1
			[27]	TE, AT, TP	4.1, 4.3, 4.4
			[14]	TE	2.4, 2.5
			[47]	TE, AT	4.4
W LXIII	62	Mg	[2]	CL, W	2.2, 4.1, 4.2
			[11]	CL, W	2.1, 2.2
			[13]	W	4.1
			[12]	W	4.1
			[27]	TE, AT, TP	4.1, 4.3, 4.4
			[31]	TE, AT, TP	4.1
			[36]	TP	4.3
			[14]	TE	2.4, 2.5
			[47]	TE, AT	4.4
W LXIV	63	Na	[2]	CL, W	2.2, 4.1, 4.2
			[11]	CL, W	2.1, 2.2
			[13]	W	4.1
			[12]	W	4.1
			[30]	TE, AT, TP	4.1
			[14]	TE	2.4, 2.5
			[47]	TE, AT	4.4
W LXV	64	Ne	[7]	CL, W	2.1, 4.1, 4.2
			[2]	CL, W	2.2, 4.1, 4.2
			[13]	W	4.1
			[12]	W	4.1
			[45]	TE, AT, TP	4.2

Table 3 (*concluded*).

Spectrum	Ion charge	Sequence	Ref.	Subject of work	Sections in text
			[14]	TE	2.4, 2.5
			[47]	TE, AT	4.4
W LXVI	65	F	[7]	CL, W	2.1, 4.1, 4.2
			[10]	CL, W, TP	2.1, 4.1
			[14]	TE	2.4, 2.5
			[47]	TE, AT	4.4
W LXVII	66	O	[7]	CL, W	2.1, 4.1, 4.2
			[10]	CL, W, TP	2.1, 4.1
			[14]	TE	2.4, 2.5
			[47]	TE, AT	4.4
W LXVIII	67	N	[7]	CL, W	2.1, 4.1, 4.2
			[10]	CL, W, TP	2.1, 4.1
			[38]	TE	4.4
			[14]	TE	2.4, 2.5
			[47]	TE, AT	4.4
			[44]	AT	4.4
W LXIX	68	C	[7]	CL, W	2.1, 4.1, 4.2
			[10]	CL, W, TP	2.1, 4.1
			[47]	TE, AT	4.4
W LXX	69	B	[7]	CL, W	2.1, 4.1, 4.2
			[10]	CL, W, TP	2.1, 4.1
			[27]	TE, AT, TP	4.1, 4.3, 4.4
			[35]	TE, AT, TP	4.4
			[47]	TE, AT	4.4
W LXXI	70	Be	[7]	CL, W	2.1, 4.1, 4.2
			[10]	CL, W, TP	2.1, 4.1
			[27]	TE, AT, TP	4.1, 4.3, 4.4
			[34]	TE, AT, TP	4.1, 4.3
			[47]	TE, AT	4.4
W LXXII	71	Li	[7]	CL, W	2.1, 4.1, 4.2
			[10]	CL, W, TP	2.1, 4.1
			[26]	TE, AT, TP	4.1
			[47]	TE, AT	4.4
W LXXIV	73	H	[43]	TP	4.4

culated emissivities of these lines using a collisional-radiative modeling and suggested experimental setup for spectroscopic diagnostics involving these lines.

5. Index to recent publications on tungsten spectra

Table 3 provides an index to the recent studies on tungsten spectra that were not included in the compilation [1]. In this table, the data contained in the indexed publications are categorized using a system of keywords similar to the one used in the NIST Atomic Spectra Bibliography Databases [106], briefly summarized below:

EL: Energy levels (experimental data);
TE: Theoretical energies;
W: Observed wavelengths (includes cases where no numerical values are given, but the wavelengths can be inferred from the given figures);
TA: Transition arrays (observations and calculations of unresolved transition arrays);
CL: Classified lines (i.e., new line identifications are given);
IP: Ionization potentials (either experimental or theoretical);
ZE: Zeeman effect (includes Landé factors);
SE: Stark effect (includes polarizabilities);
PT: Parametric theory;
AT: Ab initio theory;
TP: Transition probabilities (either experimental or theoretical; includes lifetimes).

6. Conclusions

Several tens of experimental and theoretical studies on various spectra of tungsten have been critically reviewed. Systematic shifts were found in some of the measurements included in the previous compilation [1]. These data have been corrected. Based on newly published high-precision calculations, some older data omitted in [1] have been confirmed and assessed. Based on an isoelectronic interpolation of previously published experimental and theoretical data, the energy of the $1s^2 2p_{1/2}$ level of Li-like W^{71+} has been derived with an uncertainty of ± 300 cm^{-1}.

As a result, the data on multiply-ionized tungsten summarized in the previous compilation [1] have been largely revised

and extended. New and revised tables of spectral lines and energy levels of 33 spectra of tungsten (Li-like through As-like, Pd-like, and Pm-like) have been constructed on the basis of new observations and calculations. These critically evaluated data greatly enhance possibilities for diagnostics of tungsten in hot plasmas of fusion reactors.

A few problems existing in experimental and theoretical studies of tungsten spectra have been outlined. One of the problems is incompleteness of spectroscopic designations of transitions and energy levels. Such incompleteness often leads to ambiguities in interpretation of observed spectral features. To avoid ambiguities, the description of energy levels must include complete sets of quantum numbers, including intermediate moments describing the genealogy of summation of electronic subshells. In complex spectra, the energy levels are often highly mixed by strong configuration interactions. In such cases the description of the energy levels must include the percentage compositions of the dominant basis states.

Another problem relates to the wavelength (or energy) calibration procedures in the measurements of spectral lines. In some cases, errors in these procedures resulted in large systematic errors in the measured wavelengths. The calibration procedures must be carefully and completely described in the presentation of experimental data.

Theoretical methods of calculation of atomic spectra have experienced a rapid progress in recent years. The accuracy of calculations employing relativistic multiconfiguration and many-body perturbation methods has greatly improved. Nevertheless, for very complex spectra of heavy atomic ions such as Pm-like W^{13+}, the accuracy of calculated atomic properties is still insufficient for unambiguous identification of observed spectra. In such complex cases, collisional-radiative modeling of intensities of spectral lines is required in addition to accurately calculated energy levels, transition rates, and collisional cross-sections.

Note added in print. After this article was submitted for publication, Sapirstein and Cheng [107] have published their extensive *S*-matrix calculations of energies of the $2p_{1/2}$ and $2p_{3/2}$ states of Li-like ions for $Z = 10$–100. Their result for the $2p_{1/2}$ level of Li-like tungsten is 193.44(3) eV, which is 0.14 eV higher than the value derived by interpolation in Sect. 2.1, 193.30(4) eV.

Acknowledgments

The author is grateful to J. Reader, Yu. Ralchenko, J.D. Gillaspy, and J.N. Tan for providing their data on observed wavelengths and calculated energy levels of Ca-like through Co-like tungsten prior to publication, and for helpful discussions on the details of microcalorimeter measurements. Helpful discussions with P. Beiersdorfer, J. Clementson, A.S. Safronova, and E. Träbert are also gratefully acknowledged. This work is supported in part by the Office of Fusion Energy Sciences of the US Department of Energy, grant No. ER54293.

References

1. A.E. Kramida and T. Shirai. At. Data Nucl. Data Tables, **95**, 305 (2009). doi:10.1016/j.adt.2008.12.002; A.E. Kramida and T. Shirai. At. Data Nucl. Data Tables, **95**, 1051 (2009). doi:10.1016/j.adt.2009.06.004.
2. J. Clementson and P. Beiersdorfer. Phys. Rev. A, **81**, 052509 (2010). doi:10.1103/PhysRevA.81.052509.
3. J. Clementson, P. Beiersdorfer, G.V. Brown, and M.F. Gu. Phys. Scr. **81**, 015301 (2010). doi:10.1088/0031-8949/81/01/015301.
4. J. Clementson, P. Beiersdorfer, and M.F. Gu. Phys. Rev. A, **81**, 012505 (2010). doi:10.1103/PhysRevA.81.012505.
5. J. Clementson, P. Beiersdorfer, E.W. Magee, H.S. McLean, and R.D. Wood. J. Phys. B, **43**, 144009 (2010). doi:10.1088/0953-4075/43/14/144009.
6. J. Clementson. Dissertation. University of Lund, Physics Dept., Lund, Sweden. 2010. p. 228.
7. J. Clementson, P. Beiersdorfer, G.V. Brown, M.F. Gu, H. Lundberg, Y. Podpaly, and E. Träbert. Can. J. Phys. **89**, 571 (2011). doi:10.1139/p11-028.
8. G.C. Osborne, A.S. Safronova, V.L. Kantsyrev, U.I. Safronova, P. Beiersdorfer, K.M. Williamson, M.E. Weller, and I. Shrestha. Can. J. Phys. **89**, 599 (2011). doi:10.1139/p11-026.
9. Yu. Ralchenko, I.N. Draganić, D. Osin, J.D. Gillaspy, and J. Reader. Phys. Rev. A **83**, 032517 (2011). doi:10.1103/PhysRevA.83.032517. Tables of energy levels of the ground configurations of K-like through Co-like W, calculated in this work by means of the FAC code, were privately communicated to the author.
10. Y. Podpaly, J. Clementson, P. Beiersdorfer, J. Williamson, G.V. Brown, and M.F. Gu. Phys. Rev. A, **80**, 052504 (2009). doi:10.1103/PhysRevA.80.052504.
11. J.D. Gillaspy, I.N. Draganić, Yu. Ralchenko, J. Reader, J.N. Tan, J.M. Pomeroy, and S.M. Brewer. Phys. Rev. A, **80**, 010501 (2009). doi:10.1103/PhysRevA.80.010501.
12. C. Biedermann, R. Radtke, R. Seidel, and T. Pütterich. Phys. Scr. **T134**, 014026 (2009). doi:10.1088/0031-8949/2009/T134/014026.
13. C. Biedermann and R. Radtke. AIP Conf. Proc.**1125**, 107 (2009). doi:10.1063/1.3141684.
14. T. Pütterich, R. Neu, R. Dux, A.D. Whiteford, M.G. O'Mullane, and the ASDEX Upgrade Team. Plasma Phys. Contr. Fusion, **50**, 085016 (2008). doi:10.1088/0741-3335/50/8/085016.
15. P. Palmeri, P. Quinet, V. Fivet, É. Biémont, H. Nilsson, L. Engström, and H. Lundberg. Phys. Scr. **78**, 015304 (2008). doi:10.1088/0031-8949/78/01/015304.
16. H. Nilsson, L. Engström, H. Lundberg, P. Palmeri, V. Fivet, P. Quinet, and É. Biémont. Eur. Phys. J. D, **49**, 13 (2008). doi:10.1140/epjd/e2008-00131-2.
17. J.-F. Wyart. J. Phys. B, **43**, 074018 (2010). doi:10.1088/0953-4075/43/7/074018.
18. M.J. Vilkas, Y. Ishikawa, and E. Träbert. Phys. Rev. A, **77**, 042510 (2008). doi:10.1103/PhysRevA.77.042510.
19. S. Wu and R. Hutton. Can. J. Phys. **86**, 125 (2008). doi:10.1139/P07-162.
20. V. Jonauskas, R. Kisielius, A. Kynienė, S. Kučas, and P.H. Norrington. Phys. Rev. A, **81**, 012506 (2010). doi:10.1103/PhysRevA.81.012506.
21. S. Kučas, R. Karazija, V. Jonauskas, and A. Momkauskaitė. J. Phys. B, **42**, 205001 (2009). doi:10.1088/0953-4075/42/20/205001.
22. P. Quinet, V. Vinogradoff, P. Palmeri, and É. Biémont. J. Phys. B, **43**, 144003 (2010). doi:10.1088/0953-4075/43/14/144003.
23. É. Biémont, P. Palmeri, and P. Quinet. J. Phys. B, **43**, 074010 (2010). doi:10.1088/0953-4075/43/7/074010.
24. R. Karpuškienė, O. Rancova, and P. Bogdanovich. J. Phys. B, **43**, 085002 (2010). doi:10.1088/0953-4075/43/8/085002.

25. G. Gaigalas, Z. Rudzikas, E. Gaidamauskas, P. Rynkun, and A. Alkauskas. Phys. Rev. A, **82**, 014502 (2010). doi:10.1103/PhysRevA.82.014502.
26. U.I. Safronova, A.S. Safronova, and W.R. Johnson. J. Phys. B, **43**, 144001 (2010). doi:10.1088/0953-4075/43/14/144001.
27. U.I. Safronova and A.S. Safronova. J. Phys. B, **43**, 074026 (2010). doi:10.1088/0953-4075/43/7/074026.
28. U.I. Safronova and M.S. Safronova. J. Phys. B, **43**, 074025 (2010). doi:10.1088/0953-4075/43/7/074025.
29. U.I. Safronova and A.S. Safronova. Can. J. Phys. **87**, 83 (2009). doi:10.1139/P08-096.
30. U.I. Safronova, A.S. Safronova, and P. Beiersdorfer. At. Data Nucl. Data Tables, **95**, 751 (2009). doi:10.1016/j.adt.2009.04.001.
31. U.I. Safronova, A.S. Safronova, and P. Beiersdorfer. J. Phys. B, **42**, 165010 (2009). doi:10.1088/0953-4075/42/16/165010.
32. U.I. Safronova, A.S. Safronova, and P. Beiersdorfer. Phys. Rev. A, **77**, 032506 (2008). doi:10.1103/PhysRevA.77.032506.
33. M.H. Chen and K.T. Cheng. J. Phys. B, **43**, 074019 (2010). doi:10.1088/0953-4075/43/7/074019.
34. K.T. Cheng, M.H. Chen, and W.R. Johnson. Phys. Rev. A, **77**, 052504 (2008). doi:10.1103/PhysRevA.77.052504.
35. J.-G. Li, P. Jönsson, C.-Z. Dong, and G. Gaigalas. J. Phys. B, **43**, 035005 (2010). doi:10.1088/0953-4075/43/3/035005.
36. H.-H. Kang, J.-G. Li, C.-Z. Dong, P. Jönsson, and G. Gaigalas. J. Phys. B, **42**, 195002 (2009). doi:10.1088/0953-4075/42/19/195002.
37. L.-Y. Xie, C.-Z. Dong, J. Jiang, J.-J. Wan, and J. Yan. Chin. Phys. B, **17**, 3294 (2008). doi:10.1088/1674-1056/17/9/025.
38. J.-Q. Li, X.-M. Zhang, M. Huang, C.-Y. Chen, and Y.-M. Zou. J. Phys. B, **43**, 035003 (2010). doi:10.1088/0953-4075/43/3/035003.
39. E.P. Ivanova. At. Data Nucl. Data Tables, **95**, 786 (2009). doi:10.1016/j.adt.2009.04.002.
40. E.P. Ivanova. Opt. Spectrosc. **107**, 1 (2009). doi:10.1134/S0030400X09070017.
41. S.A. Blundell. Can. J. Phys. **87**, 55 (2009). doi:10.1139/P08-065.
42. S.A. Blundell, W.R. Johnson, M.S. Safronova, and U.I. Safronova. Phys. Rev. A, **77**, 032507 (2008). doi:10.1103/PhysRevA.77.032507.
43. A.M. Puchkov and L.N. Labzovskiĭ. Opt. Spectrosc. **106**, 153 (2009). doi:10.1134/S0030400X09020015.
44. X.-L. Wang, W.-L. Lu, X. Gao, and J.-M. Li. Chin. Phys. Lett. **26**, 043101 (2009). doi:10.1088/0256-307X/26/4/043101.
45. M.J. Vilkas, J.M. López-Encarnación, and Y. Ishikawa. At. Data Nucl. Data Tables, **94**, 50 (2008). doi:10.1016/j.adt.2007.09.001.
46. P. Mandelbaum and J.L. Schwob. Eur. Phys. J. D, **49**, 173 (2008). doi:10.1140/epjd/e2008-00159-2.
47. U. Feldman, J.E. Seely, E. Landi, and Yu. Ralchenko. Nucl. Fusion, **48**, 045004 (2008). doi:10.1088/0029-5515/48/4/045004.
48. Y.-J. Rhee and D.-H. Kwon. Int. J. Mass Spectrom. **271**, 45 (2008). doi:10.1016/j.ijms.2007.10.009.
49. J.P. Desclaux. Int. J. Mass Spectrom. **271**, 30 (2008). doi:10.1016/j.ijms.2007.10.014.
50. E. Charro, Z. Curiel, and I. Martín. Int. J. Quantum Chem. **108**, 744 (2008). doi:10.1002/qua.21552.
51. S.A. Blundell. Phys. Rev. A, **47**, 1790 (1993). doi:10.1103/PhysRevA.47.1790. PMID:9909131.
52. V.A. Yerokhin, A.N. Artemyev, and V.M. Shabaev. Phys. Rev. A, **75**, 062501 (2007). doi:10.1103/PhysRevA.75.062501.
53. A.E. Kramida and M.-C. Buchet-Poulizac. Eur. Phys. J. D, **39**, 173 (2006). doi:10.1140/epjd/e2006-00122-3.
54. W.C. Martin and R. Zalubas. J. Phys. Chem. Ref. Data, **9**, 1 (1980). doi:10.1063/1.555617.
55. W.C. Martin, R. Zalubas, and A. Musgrove. J. Phys. Chem. Ref. Data, **14**, 751 (1985). doi:10.1063/1.555736.
56. R.J. Thomas and W.M. Neupert. Astrophys. J. Suppl. Ser. **91**, 461 (1994). doi:10.1086/191944.
57. K.G. Widing and J.D. Purcell. Astrophys. J. **204**, L151 (1976). doi:10.1086/182076.
58. S. Suckewer, J.L. Cecchi, S. Cohen, R. Fonck, and E. Hinnov. Phys. Lett. A, **80**, 259 (1980). doi:10.1016/0375-9601(80)90016-X.
59. E. Hinnov, B. Denne, the TFTR Operating Team, and the JET Operating Team. Phys. Rev. A, **40**, 4357 (1989). doi:10.1103/PhysRevA.40.4357. PMID:9902676.
60. J. Sugar, V. Kaufman, and W.L. Rowan. J. Opt. Soc. Am. B, **10**, 13 (1993). doi:10.1364/JOSAB.10.000013.
61. J. Reader, J. Sugar, N. Acquista, and R. Bahr. J. Opt. Soc. Am. B, **11**, 1930 (1994). doi:10.1364/JOSAB.11.001930.
62. J. Sugar, V. Kaufman, and W.L. Rowan. J. Opt. Soc. Am. B, **9**, 344 (1992). doi:10.1364/JOSAB.9.000344.
63. U. Staude, Ph. Bosselmann, R. Büttner, D. Horn, K.-H. Schartner, F. Folkmann, A.E. Livingston, T. Ludziejewski, and P.H. Mokler. Phys. Rev. A, **58**, 3516 (1998). doi:10.1103/PhysRevA.58.3516.
64. R.J. Knize. Phys. Rev. A, **43**, 1637 (1991). doi:10.1103/PhysRevA.43.1637. PMID:9905197.
65. S. Madzunkov, E. Lindroth, N. Eklöw, M. Tokman, A. Paál, and R. Schuch. Phys. Rev. A, **65**, 032505 (2002). doi:10.1103/PhysRevA.65.032505.
66. Ph. Bosselmann, U. Staude, D. Horn, K.-H. Schartner, F. Folkmann, A.E. Livingston, and P.H. Mokler. Phys. Rev. A, **59**, 1874 (1999). doi:10.1103/PhysRevA.59.1874.
67. D. Feili, Ph. Bosselmann, K.-H. Schartner, F. Folkmann, A.E. Livingston, E. Träbert, X. Ma, and P.H. Mokler. Phys. Rev. A, **62**, 022501 (2000). doi:10.1103/PhysRevA.62.022501.
68. C. Brandau, C. Kozhuharov, A. Müller, W. Shi, S. Schippers, T. Bartsch, S. Böhm, C. Böhme, A. Hoffknecht, H. Knopp, N. Grün, W. Scheid, T. Steih, F. Bosch, B. Franzke, P.H. Mokler, F. Nolden, M. Steck, T. Stöhlker, and Z. Stachura. Phys. Rev. Lett. **91**, 073202 (2003). doi:10.1103/PhysRevLett.91.073202. PMID:12935014.
69. P. Beiersdorfer, H. Chen, D.B. Thorn, and E. Träbert. Phys. Rev. Lett. **95**, 233003 (2005). doi:10.1103/PhysRevLett.95.233003. PMID:16384304.
70. P.J. Mohr, B.N. Taylor, and D.B. Newell. Rev. Mod. Phys. **80**, 633 (2008). doi:10.1103/RevModPhys.80.633.
71. M.F. Gu. Can. J. Phys. **86**, 675 (2008). doi:10.1139/P07-197.
72. Yu. Ralchenko, I.N. Draganic, J.N. Tan, J.D. Gillaspy, J.M. Pomeroy, J. Reader, U. Feldman, and G.E. Holland. J. Phys. B, **41**, 021003 (2008). doi:10.1088/0953-4075/41/2/021003.
73. Yu. Ralchenko and Y. Maron. J. Quant. Spectrosc. Radiat. Transf. **71**, 609 (2001). doi:10.1016/S0022-4073(01)00102-9.
74. M.A. Ali and Y.-K. Kim. J. Opt. Soc. Am. B, **9**, 185 (1992). doi:10.1364/JOSAB.9.000185.
75. Yu. Ralchenko, I.N. Draganic, J.N. Tan, J.D. Gillaspy, J.M. Pomeroy, J. Reader, U. Feldman, and G.E. Holland. J. Phys. B, **41**, 021003 (2008). doi:10.1088/0953-4075/41/2/021003.
76. P. Neill, C. Harris, A.S. Shlyaptseva, S. Hamasha, S. Hansen,

P. Beiersdorfer, and U.I. Safronova. The study of X-ray M-shell spectra of W ions from the Livermore electron beam ion trap, Lawrence Livermore Lab., University of California Report UCRL-JRNL-201473, Livermore, CA. 2003.
77. P. Neill, C. Harris, A.S. Safronova, S. Hamasha, S. Hansen, U.I. Safronova, and P. Beiersdorfer. Can. J. Phys. **82**, 931 (2004). doi:10.1139/p04-053.
78. Y. Ralchenko, J.N. Tan, J.D. Gillaspy, J.M. Pomeroy, and E. Silver. Phys. Rev. A, **74**, 042514 (2006). doi:10.1103/PhysRevA.74.042514.
79. J.F. Seely, C.M. Brown, and W.E. Behring. J. Opt. Soc. Am. B, **6**, 3 (1989). doi:10.1364/JOSAB.6.000003.
80. J.F. Seely, C.M. Brown, and U. Feldman. At. Data Nucl. Data Tables, **43**, 145 (1989). doi:10.1016/0092-640X(89)90017-X.
81. S.R. Elliott, P. Beiersdorfer, B.J. MacGowan, and J. Nilsen. Phys. Rev. A, **52**, 2689 (1995). doi:10.1103/PhysRevA.52.2689. PMID:9912550.
82. R. Neu, K.B. Fournier, D. Schlögl, and J. Rice. J. Phys. B, **30**, 5057 (1997). doi:10.1088/0953-4075/30/21/036.
83. N. Tragin, J.-P. Geindre, P. Monier, J.-C. Gauthier, C. Chenais-Popovics, J.-F. Wyart, and C. Bauche-Arnoult. Phys. Scr. **37**, 72 (1988). doi:10.1088/0031-8949/37/1/011.
84. W.R. Johnson and G. Soff. At. Data Nucl. Data Tables, **33**, 405 (1985). doi:10.1016/0092-640X(85)90010-5.
85. G.W.F. Drake. Can. J. Phys. **66**, 586 (1988). doi:10.1139/p88-100.
86. T. Pütterich, R. Neu, C. Biedermann, R. Radtke, and the ASDEX Upgrade Team. J. Phys. B, **38**, 3071 (2005). doi:10.1088/0953-4075/38/16/017.
87. Yu. Ralchenko, J. Reader, J.M. Pomeroy, J.N. Tan, and J.D. Gillaspy. J. Phys. B, **40**, 3861 (2007). doi:10.1088/0953-4075/40/19/007.
88. M.B. Chowdhuri, S. Morita, M. Goto, H. Nishimura, K. Nagai, and S. Fujioka. Plasma Fusion Res. **2**, S1060 (2007). doi:10.1585/pfr.2.S1060.
89. Yu. Ralchenko, A.E. Kramida, J. Reader, and NIST ASD Team. NIST Atomic Spectra Database, v. 4.0. Available online at http://physics.nist.gov/asd. 2010.
90. J. Sugar and V. Kaufman. Phys. Rev. A, **21**, 2096 (1980). doi:10.1103/PhysRevA.21.2096.
91. C.S. Harte, C. Suzuki, T. Kato, H.A. Sakaue, D. Kato, K. Sato, N. Tamura, S. Sudo, R. D'Arcy, E. Sokell, J. White, and G. O'Sullivan. J. Phys. B, **43**, 205004 (2010). doi:10.1088/0953-4075/43/20/205004.
92. W.-Ü L. Tchang-Brillet, J.-F. Wyart, A.N. Ryabtsev, R.R. Kildiyarova, and E.Ya. Kononov. Spectra of moderately charged tungsten ions, 10th International Colloquium on Atomic Spectra and Oscillator Strengths for Astrophysical and Laboratory Plasmas (ASOS-10), 3–7 August 2010, Berkeley, CA. Poster P25.
93. R.D. Cowan. The theory of atomic structure and spectra. University of California Press, Berkeley, CA. 1981. p. 731.
94. R. Radtke, C. Biedermann, P. Mandelbaum, and J.L. Schwob. J. Phys.: Conf. Ser. **58**, 113 (2007). doi:10.1088/1742-6596/58/1/019.
95. R. Radtke, C. Biedermann, G. Fussmann, J.L. Schwob, P. Mandelbaum, and R. Doron. *In* Atomic and plasma-material interaction data for fusion. Vol. 13. *Edited by* R.E.H. Clark. International Atomic Energy Agency, Vienna. 2007. pp. 45–66.
96. A. Bar-Shalom, M. Klapisch, and J. Oreg. J. Quant. Spectrosc. Radiat. Transf. **71**, 169 (2001). doi:10.1016/S0022-4073(01)00066-8.
97. F.A. Parpia, C. Froese Fischer, and I.P. Grant. Comput. Phys. Commun. **94**, 249 (1996). doi:10.1016/0010-4655(95)00136-0.
98. R. Hutton, Y. Zou, J. Reyna Almandos, C. Biedermann, R. Radtke, A. Greier, and R. Neu. Nucl. Instrum. Methods Phys. Res. B, **205**, 114 (2003). doi:10.1016/S0168-583X(03)00543-3.
99. M.S. Safronova, W.R. Johnson, and U.I. Safronova. Phys. Rev. A, **53**, 4036 (1996). doi:10.1103/PhysRevA.53.4036. PMID:9913369.
100. M.S. Safronova, W.R. Johnson, and U.I. Safronova. Phys. Rev. A, **54**, 2850 (1996). doi:10.1103/PhysRevA.54.2850. PMID:9913799.
101. C.M. Brown, J.F. Seely, D.R. Kania, B.A. Hammel, C.A. Back, R.W. Lee, A. Bar-Shalom, and W.E. Behring. At. Data Nucl. Data Tables, **58**, 203 (1994). doi:10.1006/adnd.1994.1027.
102. M.J. Vilkas and Y. Ishikawa. Phys. Rev. A, **72**, 032512 (2005). doi:10.1103/PhysRevA.72.032512.
103. W.R. Johnson. Can. J. Phys. **89**, 429 (2011). doi:10.1139/p11-018.
104. R. Hutton, Y.-M. Zou, M. Andersson, T. Brage, and I. Martinson. J. Phys. B, **43**, 144026 (2010). doi:10.1088/0953-4075/43/14/144026.
105. J.E. Sansonetti and W.C. Martin. J. Phys. Chem. Ref. Data, **34**, 1559 (2005). doi:10.1063/1.1800011.
106. A.E. Kramida and J.R. Fuhr. NIST Atomic Spectra Bibliographic Databases, online at http://physics.nist.gov/asbib/. 2010.
107. J. Sapirstein and K.T. Cheng. Phys. Rev. A, **83**, 012504 (2011). doi:10.1103/PhysRevA.83.012504.